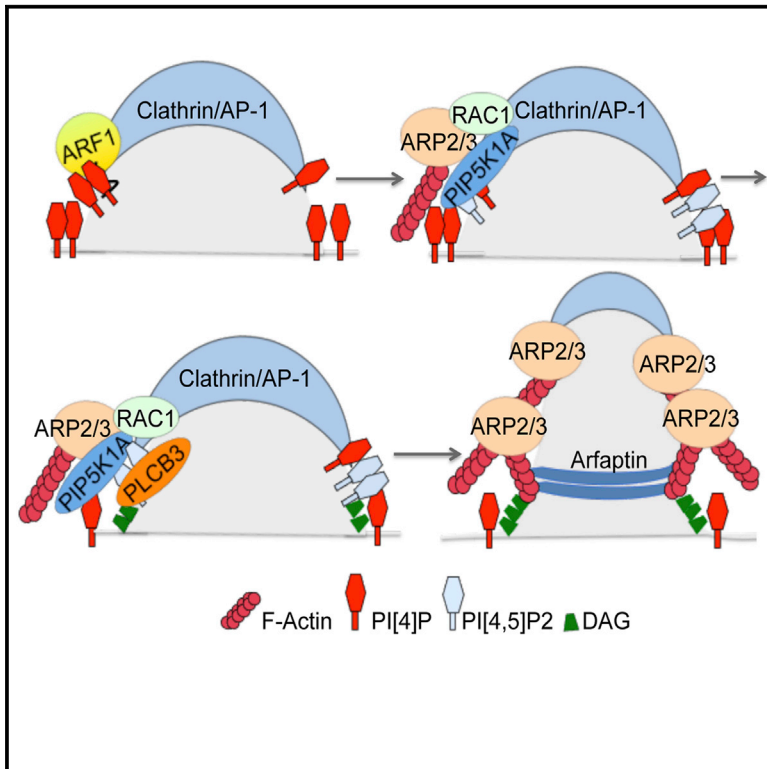


# Cell Reports

## Spatiotemporal Control of Lipid Conversion, Actin-Based Mechanical Forces, and Curvature Sensors during Clathrin/AP-1-Coated Vesicle Biogenesis

### Graphical Abstract



### Authors

Mihaela Anitei, Christoph Stange, Cornelia Czupalla, ..., Ünal Coskun, Andrej Shevchenko, Bernard Hoflack

### Correspondence

bernard.hoflack@biotec.tu-dresden.de

### In Brief

Clathrin/adaptor protein-1 (AP-1) coats control the transport of specific cargoes between the biosynthetic and endocytic pathways. Anitei et al. illustrate the coordination of protein networks controlling the biophysical properties of lipid bilayers, actin-based mechanical forces, and membrane curvature during clathrin/AP-1-coated carrier biogenesis.

### Highlights

- Clathrin/AP-1-coated vesicles mediate transport between Golgi and endosomes
- The transition between flat and curved membranes requires PI[4]P to DAG conversion
- Lipid conversion is coupled to mechanical forces provided by actin polymerization
- Membrane curvature sensors arfaptins-1/2 guide transport carrier scission



Anitei et al., 2017, Cell Reports 20, 2087–2099  
August 29, 2017 © 2017 The Authors.  
<http://dx.doi.org/10.1016/j.celrep.2017.08.013>

CellPress

# Spatiotemporal Control of Lipid Conversion, Actin-Based Mechanical Forces, and Curvature Sensors during Clathrin/AP-1-Coated Vesicle Biogenesis

Mihaela Anitei,<sup>1,7</sup> Christoph Stange,<sup>1,7</sup> Cornelia Czupalla,<sup>1</sup> Christian Niehage,<sup>1,6</sup> Kai Schuhmann,<sup>2</sup> Pia Sala,<sup>3,4</sup> Aleksander Czogalla,<sup>3,4,5</sup> Theresia Pursche,<sup>1</sup> Ünal Coskun,<sup>3,4</sup> Andrej Shevchenko,<sup>2</sup> and Bernard Hoflack<sup>1,8,\*</sup>

<sup>1</sup>Biotechnology Center, Dresden University of Technology, Tatzberg 47-49, 01307 Dresden, Germany

<sup>2</sup>Max Planck Institute of Molecular Cell Biology and Genetics, Pfotenhauerstrass 108, 01307 Dresden, Germany

<sup>3</sup>Paul Langerhans Institute Dresden of the Helmholtz Centre Munich at the University Clinic Carl Gustav Carus, TU Dresden, 01307 Dresden, Germany

<sup>4</sup>German Center for Diabetes Research (DZD e.V.), 85764 Neuherberg, Germany

<sup>5</sup>Department of Cytochemistry, University of Wrocław, Faculty of Biotechnology, Joliot-Curie 14a, 50-383 Wrocław, Poland

<sup>6</sup>Mannheim University of Applied Sciences, Instrumental Analysis, and Bioanalysis, Paul-Wittsack-Strasse 10, 68163 Mannheim, Germany

<sup>7</sup>These authors contributed equally

<sup>8</sup>Lead Contact

\*Correspondence: [bernard.hoflack@biotec.tu-dresden.de](mailto:bernard.hoflack@biotec.tu-dresden.de)

<http://dx.doi.org/10.1016/j.celrep.2017.08.013>

## SUMMARY

Clathrin/adaptor protein-1-coated carriers connect the secretory and the endocytic pathways. Carrier biogenesis relies on distinct protein networks changing membrane shape at the *trans*-Golgi network, each regulating coat assembly, F-actin-based mechanical forces, or the biophysical properties of lipid bilayers. How these different hubs are spatiotemporally coordinated remains largely unknown. Using *in vitro* reconstitution systems, quantitative proteomics, and lipidomics, as well as *in vivo* cell-based assays, we characterize the protein networks controlling membrane lipid composition, membrane shape, and carrier scission. These include PIP5K1A and phospholipase C- $\beta$  3 controlling the conversion of PI[4]P into diacylglycerol. PIP5K1A binding to RAC1 provides a link to F-actin-based mechanical forces needed to tubulate membranes. Tubular membranes then recruit the BAR-domain-containing arfaptin-1/2 guiding carrier scission. These findings provide a framework for synchronizing the chemical/biophysical properties of lipid bilayers, F-actin-based mechanical forces, and the activity of proteins sensing membrane shape during clathrin/adaptor protein-1-coated carrier biogenesis.

## INTRODUCTION

In mammalian cells, clathrin and adaptor protein-1 (AP-1) coats mediate the trafficking of specific cargoes between the biosynthetic and endocytic pathways. These cargoes include the mannose 6-phosphate receptors (MPRs) and their bound newly synthesized lysosomal enzymes, trafficking between the *trans*-Golgi network (TGN) and the endolysosomal system to maintain

cell homeostasis (Ghosh et al., 2003; Le Borgne and Hoflack, 1998). They also include signaling receptors such as Notch/Delta regulating cell differentiation and tissue organization (Le Borgne, 2006).

Clathrin/AP-1 coat assembly onto flat membranes relies on the recognition of a mosaic of membrane components, comprising phosphatidylinositol-4 phosphate (PI[4]P), sorting signals present in the cytoplasmic domains of their specific cargoes, and the small GTPase ADP ribosylation factor 1 (ARF1) (Baust et al., 2006; Traub and Bonifacino, 2013). The next stage involves mechanisms allowing flat membranes to change their shape into bended structures. This involves not only coats, but also ENTH/ANTH-domain-containing proteins (Legendre-Guillemin et al., 2004) able to insert an amphipathic helix into the cytosolic leaflet of lipid bilayers, as also does the ARF1 GTPase (Lundmark et al., 2008), increasing lipid bilayer asymmetry and mechanically bending membranes. Changes in membrane shape also require mechanical forces provided by actin polymerization (Anitei and Hoflack, 2011; Anitei et al., 2010). Clathrin/AP-1 coat assembly initiates the recruitment of actin nucleation promoting factors, which, upon activation by the RAC1 GTPase, promote ARP2/3-dependent actin polymerization toward membranes, thereby providing forces able to overcome membrane rigidity (Anitei et al., 2010; Kaksonen et al., 2006). Filamentous actin (F-actin)-based forces generate tubular membrane structures onto which curvature-sensitive Bin-Amphiphysin-Rvs (BAR) domain proteins can be recruited, as seen during endocytosis (Qualmann et al., 2011).

The transition from flat to curved membranes also entails lipid modifications and a reorganization of lipid bilayers. These modifications engage phosphoinositides (PIPs), which provide membrane identity and are selectively recognized by PIP-interacting proteins that sustain carrier formation (Di Paolo and De Camilli, 2006). On the other hand, the biosynthesis of conical lipids such as diacylglycerol (DAG), phosphatidic acid (PA), or lysophospholipids changes the biophysical properties of lipid bilayers inducing membrane curvature (Haucke and Di Paolo, 2007).





How coat assembly, modifications in the biochemical and biophysical properties of lipid bilayers and F-actin-based forces are spatiotemporally coordinated during a single step of membrane traffic to change membrane shape, and how these changes are sensed by proteins controlling later events of carrier biogenesis, remain poorly understood. Here, we identify and illustrate the functional importance of the protein networks that spatiotemporally coordinate biochemical, biophysical, and mechanical reactions during clathrin/AP-1-coated carrier biogenesis.

## RESULTS

### Protein Networks Enriched on Flat and Tubular Clathrin/AP-1-Coated Membranes

To identify the protein networks regulating the different stages of clathrin/AP-1-coated transport carrier biogenesis, we used synthetic membrane biology and quantitative mass-spectrometry-based proteomics. Synthetic liposomes containing PI[4]P and the cytoplasmic domain of an AP-1 cargo (the varicella zoster virus gE/gpI protein) preferentially recruit clathrin/AP-1 coats from mouse brain cytosolic extracts in the presence of GTP $\gamma$ S (Baust et al., 2006). In the presence of ATP, actin polymerization occurs, and flat GUV membranes form tubular projections (Anitei et al., 2010) (Figures 1A and 1B) recapitulating clathrin/AP-1-coated carrier biogenesis in live cells (Waguri et al., 2003). We used O<sup>18</sup>/O<sup>16</sup> labeling during trypsin digestion (Figures 1B and 1C) and label free quantitative analysis (Figure S1B) to identify proteins selectively recruited onto flat versus tubular clathrin/AP-1-coated membranes (Figure 1C; Table S1) and enriched on clathrin/AP-1-coated versus non-coated membranes (Figure S1B; Table S2), respectively. Pathway enrichment analysis (Figures 1D and S1A; Table S1) showed that the proteins recruited onto flat membranes (no ATP) were mostly associated with TGN- and lysosome-associated trafficking pathways and included coat components (i.e., clathrin and AP-1 subunits), PI[4]-kinase beta (PI4KB) (Baust et al., 2006), which generates PI[4]P from PI (Godi et al., 1999), and casein kinase II (CSK2B/CSNK2B), which phosphorylates MPR cytoplasmic tails and AP-1 at the TGN (Mésesse et al., 1990; Doray et al., 2002; Mésesse and Hoflack, 1993) (Figure S1A). In contrast, tubular membranes (incubated with ATP) recruited components of the actin cytoskeleton regulatory pathway (e.g., RAC1, ARP2/3 complex subunits, the ARP2/3 regulatory Wiskott-Aldrich syndrome-like protein [WASL], and p21 protein [Cdc42/Rac]-activated kinases [PAKs]), as well as components of the phospholipid metabolism pathway [i.e., the PI[4]P 5-kinases type I alpha [PIP5K1A/PI51A], beta, and gamma, which produce PI[4,5]P2] (Figures 1C and 1D). On clathrin/AP-1-coated liposomes, we have also identified phospholipases beta 1 (PLCB1) and 3 (PLCB3) (Díaz Añel, 2007), enzymes that can hydrolyze PI[4,5]P2 (Figure S1B; Table S2). Western blot analysis confirmed the enrichments of RAC1, PIP5K1A, and PLCB3 on tubular membranes and indicated a preferential recruitment of the Golgi-localized BAR domain proteins arfaptin-2 (ARFP2) (Man et al., 2011; Cruz-Garcia et al., 2013) and arfaptin-1 (Kano et al., 1997) (Figures 1E and 1F). Latrunculin B, an actin polymerization inhibitor, significantly reversed the enrichment of PIP5K1A, PLCB3, RAC1, and arfaptin-1/2, indicating that actin-dependent membrane

tubulation, and not ATP alone, was necessary for their recruitment (Figures 1E and 1F). In conclusion, an increase in clathrin/AP-1-coated membrane curvature coincides with the recruitment of PIP converting enzymes, of the machinery for RAC1-dependent actin polymerization, and of arfaptins sensing and/or imposing membrane curvature.

### PIP5K1A and PLCB3 Control DAG Synthesis and Clathrin/AP-1 Carrier Biogenesis

We next investigated if PIP5K1A and PLCB3 played any role in clathrin/AP-1-coated carrier biogenesis in cells. The small interfering RNA (siRNA)-mediated knock down of PIP5K1A or PLCB3 in HeLa cells stably expressing GFP-tagged CIMPR tail made of the CIMPR transmembrane and cytoplasmic domains (GFP-MPR) (Waguri et al., 2003) caused a fragmentation of the GFP-MPR-rich TGN, without affecting AP-1 coat association with membranes (Figures 2A, 2B, 2E, and S2A). Time-lapse microscopy showed that PIP5K1A or PLCB3 depletion significantly reduced the formation of post-TGN GFP-MPR-containing tubules connecting the biosynthetic and endocytic pathways (Waguri et al., 2003) (Figures 2C and 2D; Movie S1). Thus, PIP5K1A and PLCB3, although not critical for clathrin/AP-1 coat assembly, were rate-limiting for clathrin/AP-1-coated carrier biogenesis, possibly by locally modifying the lipid composition of the membrane. Using a specific antibody, we could detect PI[4,5]P2 in the GFP-MPR<sup>+</sup> *trans*-Golgi region, but in low amounts (Figure 2E). This could be due to its hydrolysis by PI[4,5]P2 phosphatases or by PLCs. Indeed, depletion of PLCB3 significantly increased the amount of PI[4,5]P2 co-detected with GFP-MPR in the peri-nuclear region, in contrast, PI[4,5]P2 was reduced to control levels in cells treated with both siPIP5K1A and siPLCB3, thereby illustrating the importance of these two enzymes (Figures 2E–2G). By fluorescence microscopy, PIP5K1A was detectable at multiple locations in the cell, including the peri-nuclear GFP-MPR<sup>+</sup> area (Figure 2H), and PLCB3 was detected on subdomains of the GFP-MPR<sup>+</sup> structures in the TGN region (Figure 2I). These data indicate that PIP5K1A and PLCB3 could contribute to lipid metabolism on Golgi membranes; i.e., by converting PI[4]P into PI[4,5]P2 and PI[4,5]P2 into DAG, respectively.

To test this hypothesis, we used HEK cells stably expressing the yellow-fluorescent protein (YFP)-tagged DAG-binding C1 domain of protein kinase C beta (YFP-DBD) (Gallegos et al., 2006). This DAG sensing probe bound Golgi membranes (Baron and Malhotra, 2002), where it co-localized with GM130 and RFP-MPR and on TGN-derived tubules carrying red fluorescent protein (RFP)-MPR (Figure S2B). Depletion of either PIP5K1A or PLCB3 significantly reduced the amount of Golgi-bound YFP-DBD (Figures 3A and 3B). The addition of the DAG analog phorbol 12,13-dibutyrate (PDBu) to PIP5K1A- and PLCB3-depleted cells partially reversed TGN fragmentation and increased GFP-MPR tubule formation (Figures 3C–3E). Thus, PIP5K1A and PLCB3 may contribute to MPR trafficking by controlling DAG production from PI[4]P.

To test if PI[4]P was required for DAG synthesis on Golgi membranes, we used the acute PI[4]P depletion system (Szentpetery et al., 2010) in which the monomeric RFP (mRFP)-tagged 12 kD FK506-binding protein (mRFP-FKBP12), alone or fused to the

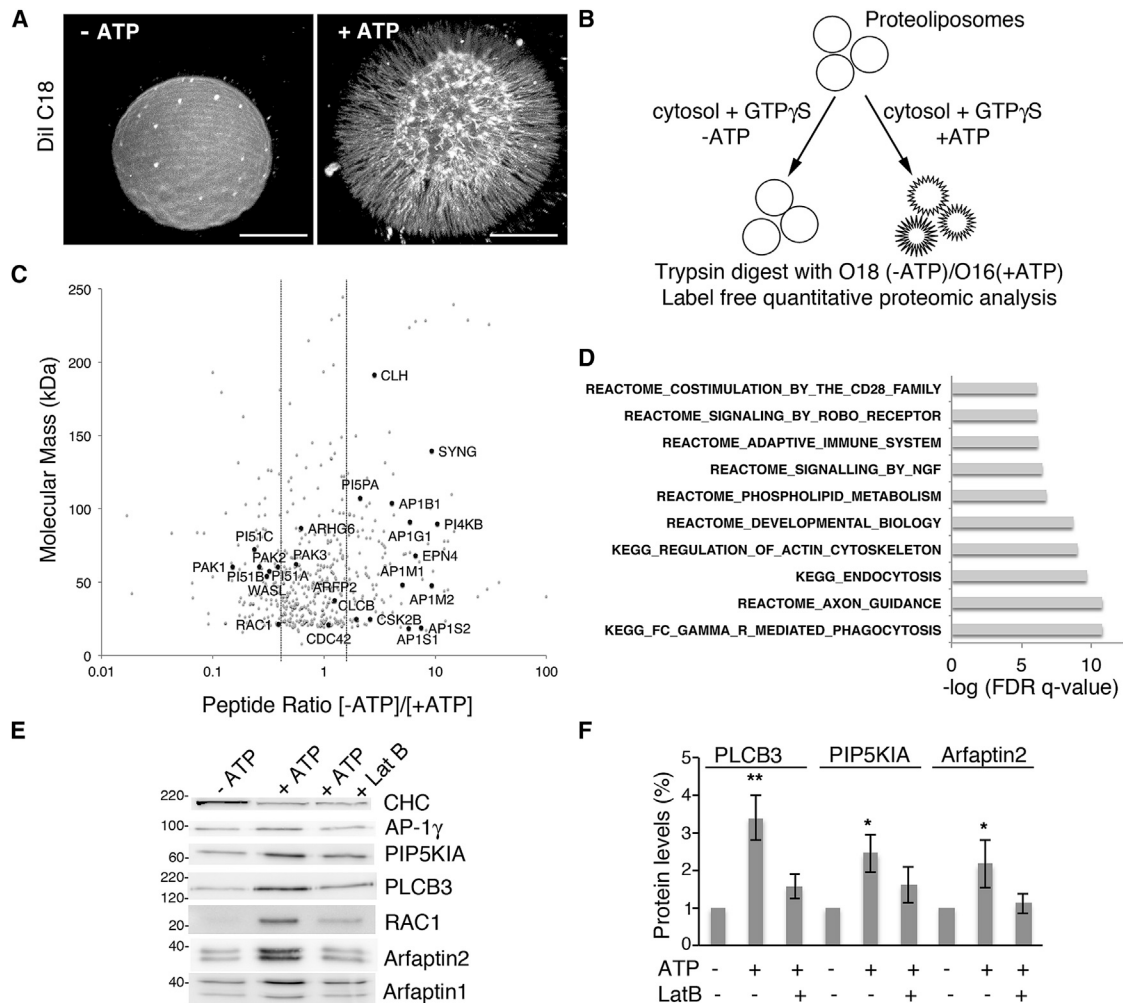


**Figure 1. Identification of Proteins Enriched on Tubular Membranes during Clathrin/AP-1 Carrier Biogenesis**

(A and B) GUVs (A) or liposomes (B) containing a gE/gpl cd peptide, PI[4]P, and the lipid dye Dil-C18 (A) were incubated with mouse brain cytosol, GTP $\gamma$ S, and without or with ATP triggering membrane tubulation (on  $54 \pm 10\%$  of GUVs;  $n = 6$  independent experiments;  $>100$  GUVs; and mean  $\pm$  SD). Scale bars, 10  $\mu$ m. (B) Liposomes were purified by floatation, and bound proteins were separated by SDS-PAGE. Gel slices were cut out and in-gel trypsin digested in the presence of either H<sub>2</sub>O<sup>16</sup> (+ATP) or H<sub>2</sub>O<sup>18</sup> (-ATP). Tryptic peptides of the corresponding gel slices were pooled and analyzed by liquid chromatography-tandem mass spectrometry (LC-MS/MS). The intensity ratios between heavy (<sup>18</sup>O) and light (<sup>16</sup>O) peptides were calculated.

(C) Proteins with a ratio -ATP/+ATP  $\geq 1.6$  were considered as enriched on flat membranes, whereas those with a ratio -ATP/+ATP  $\leq 0.4$  as enriched on tubular membranes (Table S1). Vertical lines indicate the 0.4 and 1.6 thresholds. Selected hits are indicated with their corresponding UniProt entry names.

(D) Pathway enrichment of the proteins preferentially recruited onto liposomes incubated with ATP was calculated using the gene set enrichment analysis (GSEA) (Mootha et al., 2003; Subramanian et al., 2005). The false discovery rate (FDR) q-value was calculated for each set.

(E and F) Liposomes containing gE/gpl cd peptide and PI[4]P were incubated with HeLa cell cytosol, GTP $\gamma$ S, with or without ATP, and with or without 20  $\mu$ M latrunculin B (LatB). Recruited proteins were analyzed by western blotting using the respective antibodies (E) and quantified using ImageJ (F) (mean  $\pm$  SD;  $n = 4$  independent experiments; \*\* $p < 0.005$ ; \* $p < 0.05$ ; significance was calculated using one-way ANOVA).

PI[4]P phosphatase Sac1 (mRFP-FKBP12-Sac1), and the CFP-tagged FKBP12-rapamycin-binding (FRB) domain fused to the *trans*-Golgi membrane protein TGN38 were expressed in cells. Upon rapamycin treatment, CFP-FRB-TGN38 recruits mRFP-FKBP12-Sac1 on the Golgi, thus leading to the acute depletion of PI[4]P. This depletion was monitored using the GFP-tagged PH domain of FAPP1 (GFP-PH-FAPP1) that binds to PI[4]P (Figure 3F). Acute PI[4]P depletion significantly reduced the binding of both GFP-PH-FAPP1 (Figures 3F and 3I) and YFP-DBD onto Golgi membranes (Figures 3G and 3J). Such changes were not

observed in cells expressing control mRFP-FKBP12 without the PI[4]P phosphatase Sac1. Thus, PI[4]P is a significant source of DAG on Golgi membranes. In addition to PI[4]P, several biosynthetic pathways control DAG production (Figure S3A), and we tested their relative contributions to GFP-MPR transport (Figures S3B–S3I). First, ARF1-dependent PLD, a PI[4,5]P<sub>2</sub>-activated enzyme produces PA, a source of DAG, from phosphatidylcholine (PC) (Sciorra et al., 1999; Brown et al., 1993). However, depletion of PLD1 or PLD2 did not significantly reduce YFP-DBD binding to the Golgi or GFP-MPR tubule formation. On the contrary, PLD2

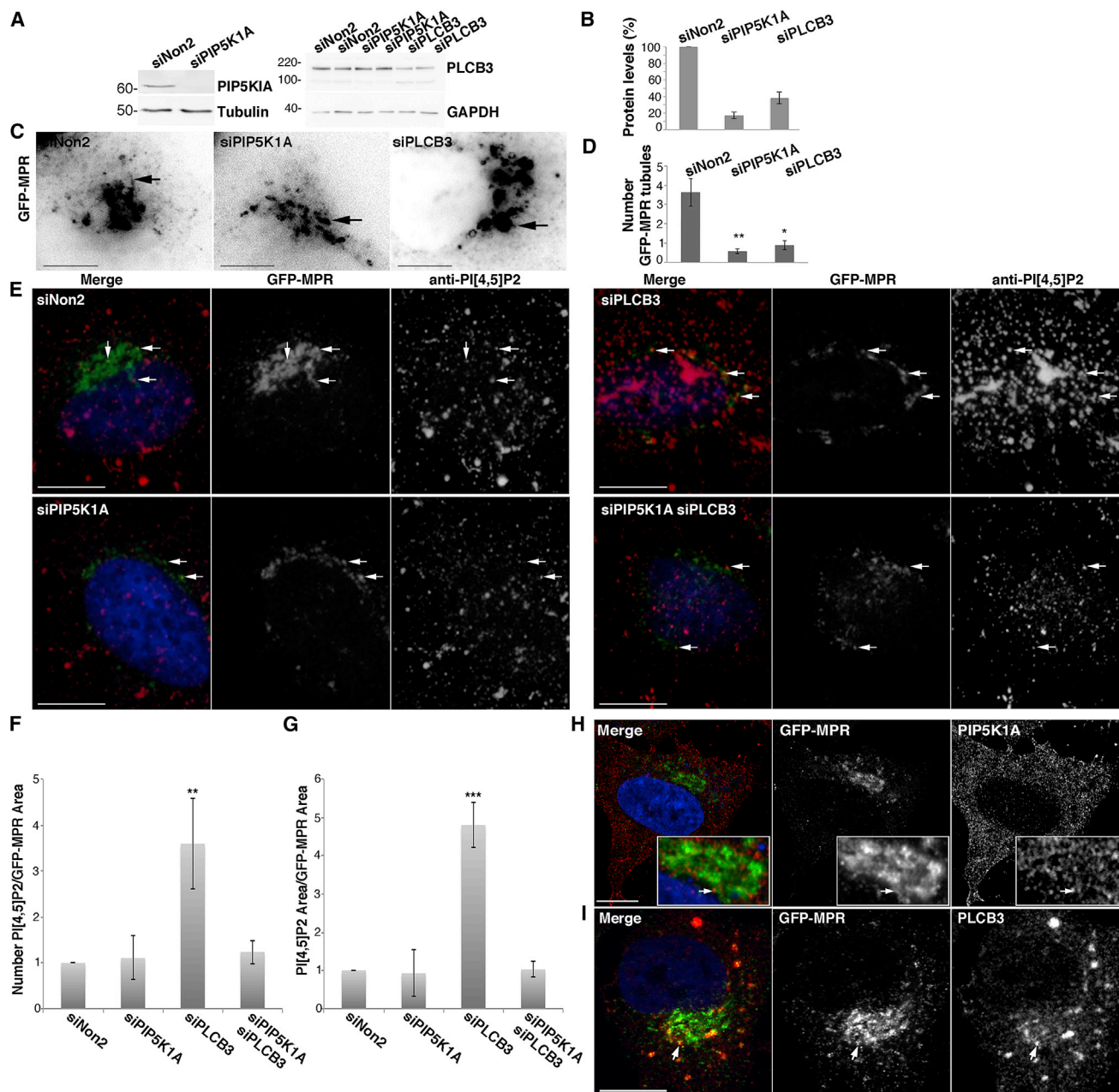


**Figure 2. PIP5KA and PLCB3 Regulate Clathrin/AP-1 Carrier Biogenesis**

(A and B) Efficiency of PIP5K1A and PLCB3 depletion was evaluated by western blot (A) and quantified using ImageJ (B) ( $n = 3$ ).

(C) GFP-MPR-expressing cells treated with siNon2, siPIP5K1A, or siPLCB3 for 72 hr were analyzed by live cell imaging (2 min; 0.5 s per frame; [Movie S1](#)). The images were inverted.

(D) The numbers of TGN-derived tubules formed per cell during 2 min were quantified ( $n = 3$ ; \* $p < 0.01$ ; \*\* $p < 0.001$ ; and  $>50$  cells/condition).

(E) GFP-MPR-expressing cells treated with the indicated siRNAs for 72 hr were fixed, co-labeled with an antibody against PI[4,5]P2 (red), and analyzed by confocal microscopy. The arrows indicate PI[4,5]P2 punctate structures localized in the GFP-MPR<sup>+</sup> peri-nuclear area.

(F and G) PI[4,5]P2 localization in the GFP-MPR<sup>+</sup> area was quantified using ImageJ. Images represent 3D volume views of image z stacks. The number of PI[4,5]P2 objects in the GFP-MPR area (F) and the ratio between the (PI[4,5]P2 area)/(GFP-MPR area) (G), relative to control, are shown.  $n = 4$  independent experiments;  $>100$  cells per condition;  $p$  value<sub>siPLCB3</sub> = 0.0031 (F); and  $p$  value<sub>siPLCB3</sub> = 0.00055 (G).

(H and I) GFP-MPR-expressing HeLa cells were co-labeled with antibodies against PIP5K1A (H, red) or PLCB3 (I, red). The arrows indicate PIP5K1A (H, inset) or PLCB3 (I) localized to the GFP-MPR<sup>+</sup> TGN. Scale bars, 10  $\mu$ m.

Data are shown as mean  $\pm$  SD (B and D) and median  $\pm$  SD (F and G).



knock down increased the number of GFP-MPR tubules ( $6.44 \pm 0.56$  tubules per cell in 2 min; mean  $\pm$  SD) compared to control ( $4.56 \pm 0.47$ ), consistent with its suggested role in carrier scission (Yang et al., 2008) (Figures S3J and S3K). Second, PA originating from other sources, such as lysophosphatidic acid (LPA), might as well contribute to DAG synthesis on the Golgi (Schmidt and Brown, 2009) (Figure S3A). Depletion of PPAP2A, a LPA and PA phosphatase (Smyth et al., 2003) important for MPR trafficking (Anitei et al., 2014), significantly reduced both YFP-DBD binding to Golgi membranes and the number of TGN-derived GFP-MPR tubules (Figures S3D–S3H). Third, sphingomyelin (SM) synthases convert ceramide and PC into DAG and SM (Huitema et al., 2004) (Figure S3A). Cell treatment with fumonisin B1, an inhibitor of this pathway, reduced the amount of DAG on the Golgi, as previously shown (Baron and Malhotra, 2002; Wang et al., 1991) (Figures S3D and S3E), without altering the recruitment of the PI[4]P-binding GFP-PH-FAPP1 (Figure S3F). Fumonisin B1 reduced the number of GFP-MPR tubules compared to control (Figures S3G and S3H; Movie S2), but to a lower degree compared to the depletion of PIP5K1A or PLCB3 (Figure 2D, above). Ceramide is transported from the endoplasmic reticulum (ER) to the Golgi by the ceramide transfer protein CERT (Hanada et al., 2009), which has a PI[4]P-binding PH domain (Fugmann et al., 2007), and could thus link DAG and PI[4]P metabolism (Figure S3A). However, CERT recruitment to the Golgi was not significantly affected after a short-term, acute PI[4]P depletion (Figures 3H and 3K) or by PIP5K1A or PLCB3 knockdown (Figure S3L). Together, these data indicate that several pathways, including a PI[4]P-dependent mechanism, contribute, albeit to different extents, to DAG synthesis on Golgi membranes during clathrin/AP-1 carrier budding.

### PI[4]P-Derived DAG Production on Synthetic Membranes

We then investigated whether the PI[4]P to DAG conversion on Golgi membranes could be recapitulated *in vitro*. We used two types of clathrin/AP-1-coated liposomes, the first one containing a mixture of PC, phosphatidylethanolamine (PE), phosphatidylserine (PS), cholesterol, and PI[4]P (as in Figure 1C, above), and the second one, in which PC, a potential PI[4]P-independent DAG source (Baron and Malhotra, 2002), was replaced by SM. Liposomes were incubated with GTP $\gamma$ S and cytosol from HEK cells stably expressing either GFP-tagged PI[4,5]P2-sensing PH domain of PLC- $\delta$  (GFP-PH-PLC $\delta$ ) (Stauffer et al., 1998) or the DAG-binding YFP-DBD. Liposomes were pelleted and analyzed by western blotting, and the amounts of recruited proteins were quantified. In the presence of ATP, PIP5K1A, PLCB3, and the probes sensing PI[4,5]P2 and DAG were progressively recruited onto PC- or SM-containing synthetic membranes (Figures 4A–4B, and S4A). It is worth noting that GFP-PH-PLC $\delta$  did not bind control liposomes, but was specifically recruited to PI[4,5]P2-containing liposomes and to PI[4]P-liposomes after incubation with ATP (Figure S1C).

Lipid conversion was then analyzed by thin layer chromatography. On liposomes containing PC or SM, PI[4]P was consumed within 10 min of incubation in the presence of ATP and concomitantly DAG was detected (Figures 4C and 4D). We also used mass-spectrometry-based lipidomics to analyze the lipid composition of PC- or SM-containing liposomes (Figures

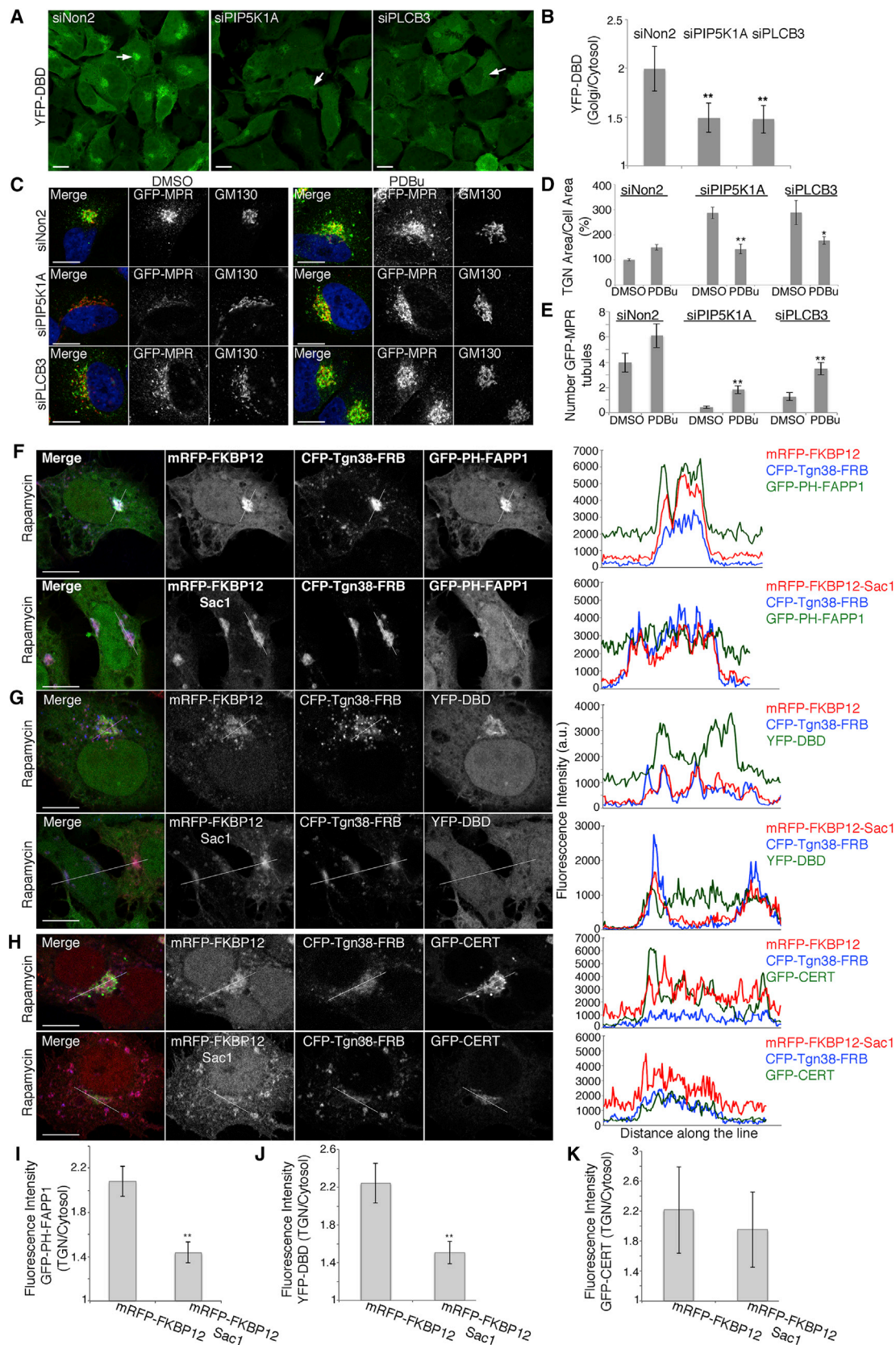
4E–4G). DAG production was readily detected, although it was slower on SM-containing when compared to PC-containing liposomes (Figures 4E and 4F). The nature of the fatty acids present in the newly produced DAG was identical to those in natural or synthetic [17:0-20:4 (37:4)] PI[4]P incorporated in liposomes (Figure 4G). Altogether, these biochemical analyses indicated that on both PC- and SM-containing clathrin/AP-1-coated liposomes, PI[4]P was a major source of DAG.

### Actin Dynamics and Lipid Metabolism Co-occur during Membrane Tubulation

We have demonstrated that PI[4]P-dependent DAG synthesis occurs during clathrin/AP-1-coated membrane tubulation *in vitro*. The question that has arisen was whether PI[4]P was actually required for membrane deformation. To examine this hypothesis, SM-containing GUVs were incubated with cytosol of HEK cells stably expressing GFP-actin, PI[4,5]P2, or DAG lipid sensors. Upon incubation with ATP, GUVs containing PI[4]P, but not control GUVs, changed their shape, switching from flat to tubular, GFP-actin-labeled structures, and PI[4,5]P2 and DAG were readily detected on their surface by GFP-PH-PLC $\delta$  and YFP-DBD (Figures 5A–5D). Tubule formation was significantly reduced when PI[4]P-containing GUVs were incubated with cytosol of PLCB3-depleted HEK cells (Figure 5D). Concomitant changes in membrane shape and lipid probe recruitment were also observed in PC-containing GUVs upon ATP addition (Figures S4B–S4E). Thus, PI[4]P, and possibly its conversion into PI[4,5]P2 and DAG, were essential for tubule elongation from GUV membranes.

### RAC1 Connects Lipid Metabolism and Actin Polymerization

We have previously shown that tubulation of clathrin/AP-1-coated membranes requires RAC1 and ARP2/3 complex-dependent actin polymerization toward membranes (Anitei et al., 2010). Therefore, the question is how these events are coordinated with the conversion of PI[4]P into DAG. DAG synthesis, through protein kinase C (PKC) recruitment and activation of PKC-dependent pathways, could modify actin dynamics; e.g., via the regulation of ARP2/3 complex localization, as observed at cell leading edges (Yang et al., 2013). However, depletion of PLCB3, while reducing the recruitment of the PKC  $\beta$  (Figure 3A, above), did not significantly modify the localization of the ARP2/3 complex subunit p34-Arc on GFP-MPR membranes (Figures S4F and S4G). On the other hand, PI[4]P significantly increased the recruitment of RAC1 on liposomes (Figure 5E). RAC1 interacts with the PI[4]P-modifying enzyme PIP5K1A (Tolias et al., 2000; Chao et al., 2010). We found that PIP5K1A and GTP-RAC1 could be co-immunoprecipitated from cells using beads coated with a GST-tagged PAK p21-binding domain (PBD) that specifically binds to active RAC1/CDC42 (Figure 5F). In addition, less GTP-RAC1 was immunoprecipitated from cell lysates after PIP5K1A depletion (Figures 5G and 5H). Conversely, the overexpression of the dominant-positive CyPet-RAC1Q71L mutant in HeLa cells triggered the formation of an enlarged AP-1-coated compartment onto which myc-PIP5K1A was heavily recruited (Figure 5I). Thus, RAC1 could recruit on membranes PIP5K1A, which could enhance RAC1- and ARP2/3-dependent actin dynamics. Accordingly, PIP5K1A



(legend on next page)



depletion reduced p34-Arc recruitment on GFP-MPR membranes, compared to control (Figures S4F and S4G). This suggests that RAC1 could provide a link between PIP5K1A recruitment, and thus lipid conversion, and ARP2/3-dependent actin polymerization during membrane tubulation.

### Arfaptins-1/2 Control Clathrin/AP-1-Coated Carrier Scission

In addition to its function in actin polymerization, RAC1 also binds the BAR domain protein family members arfaptin-1 and -2 (Shin and Exton, 2001; Cruz-Garcia et al., 2013). Arfaptin-2 was recruited on clathrin/AP-1-coated membranes (Table S2), and both arfaptin-1 and -2 were enriched upon membrane tubulation (Figures 1E and 1F, above). Since BAR domain proteins can both sense and impose membrane curvature (Qualmann et al., 2011), it was important to assess their potential contribution to clathrin/AP-1-coated membrane deformation. In HeLa cells, endogenous and fluorescent-tagged arfaptin-1 and arfaptin-2 overlapped with each other and with MPR in the TGN region and on endosomes (Figures 6A, 6B, S5A, and S5B). A subpopulation of TGN-derived tubules contained arfaptin-1 and MPR, and the arfaptin-1-containing tubules were coated by AP-1 (Figures 6A–6D; Movies S3 and S4). On artificial membranes, GFP-tagged arfaptin-2 was detected as patches on the surface of flat GUVs, but it preferentially bound to tubules projecting from GUV surfaces upon ATP addition (Figure 6E). These findings indicate that arfaptins-1 and -2 are important for clathrin/AP-1-dependent trafficking. To test this, we co-depleted arfaptin-1 and -2 in GFP-MPR-expressing cells and found that their depletion increased both the number and length of GFP-MPR-containing carriers when compared to control (Figures 6F–6I and S5C; Movies S1 and S5). Interestingly, 55% of the scission events ( $n = 32$  cells) on tubules containing mCherry-arfaptin-1 and GFP-MPR occurred at the edges of arfaptin-positive domains (Figures 6J and S5D). Thus, arfaptins-1/2 are required for the scission of clathrin/AP-1-coated carriers, but not for their biogenesis, which requires coordinated actin polymerization and PI[4]P turnover.

### DISCUSSION

We have previously illustrated how coordinated clathrin/AP-1 coat assembly and actin polymerization provide mechanical

forces required for overcoming membrane rigidity and changing membrane shape at the TGN (Anitei et al., 2010). Here, we illustrate how changes in membrane lipid composition (i.e., PI[4]P-dependent DAG synthesis), and actin-based forces are coordinated to change membrane shape, thereby allowing the binding of the BAR-domain-containing arfaptins that guide carrier scission. Altogether, these studies provide a biochemical, biophysical, and mechanical framework spatiotemporally orchestrating post-Golgi transport to the endosomal/lysosomal system.

At the TGN, PI[4]P is important for clathrin/AP-1 coat assembly (Wang et al., 2003; Baust et al., 2006). Here, we demonstrate that PI[4]P conversion to DAG, possibly via the intermediate PI[4,5]P<sub>2</sub>, occurs during clathrin/AP-1-coated carrier biogenesis. Our results suggest that PI[4]P may be converted by PIP5K1A into PI[4,5]P<sub>2</sub> that is rapidly converted by PLCB3 into DAG. This conclusion is supported by the lipidomic analysis of liposomes showing that PI[4]P and the produced DAG contain the very same unsaturated fatty acids. Such lipid conversion may be required for carrier formation, similar to how PI[4,5]P<sub>2</sub> to PI[3,4]P<sub>2</sub> conversion functions during endocytosis (Posor et al., 2013). DAG is easily detected on the Golgi, whereas PIP5K1A and PI[4,5]P<sub>2</sub> are detectable only in small amounts in the GFP-MPR<sup>+</sup> TGN region, as well as on clathrin/AP-1-coated artificial membranes in the presence of ATP and GTP $\gamma$ S. The low amounts of PI[4,5]P<sub>2</sub> on the TGN may be caused by the transient recruitment of enzymes, such as PIP5K1A caused by RAC1 activation/inactivation cycles, as seen during cell migration (Chao et al., 2010), or by PI[4,5]P<sub>2</sub> rapid modification by phosphatases or PLCs. PLCB3 is important for GFP-MPR carrier budding from the TGN, and it may also control other trafficking pathways; i.e., vesicular stomatitis virus G protein (VSV-G) post-TGN transport (Díaz Añel, 2007). Another member of the PLC family, PLC $\gamma$ 1, affects DAG production at the Golgi upon cargo arrival, but at a low degree at steady state (Sicart et al., 2014), indicating that it controls this pathway together with other PLCs (i.e., PLCB3).

Multiple metabolic pathways contribute to DAG synthesis. Our study argues that PI[4]P is a major source of DAG needed for clathrin/AP-1-coated carrier formation. While excluding the intervention of PLD1 and PLD2 in this process, our study confirms that DAG is partly derived from a PC/ceramide pathway (Baron and Malhotra, 2002), but also from PA conversion by acyltransferase PPAP2A, functionally similar to lipid phosphate

### Figure 3. PIP5KA and PLCB3 Regulate DAG Synthesis on Golgi Membranes

(A) HEK cells stably expressing YFP-DBD were treated with the indicated siRNAs and fixed after 72 hr. The arrows indicate the peri-nuclear, YFP-DBD<sup>+</sup> region.  
(B) Mean fluorescence intensities of YFP-DBD were measured on the Golgi area and in the cytosol using ImageJ. The Golgi/cytosol ratios are shown ( $n \geq 3$ ; \*\* $p \leq 0.003$ ; and  $>100$  cells/condition).  
(C) GFP-MPR-expressing cells incubated with the indicated siRNAs for 72 hr were incubated with control DMSO or with the DAG analog 0.25  $\mu$ M PDBu for 5 hr, fixed, and co-labeled with anti-GM130 antibodies (red).  
(D) The areas of the GFP-MPR<sup>+</sup> TGN and total cell areas were measured using ImageJ. The ratios (TGN area)/(total cell area) are shown for each condition ( $n = 3$ ; \*\* $p = 0.002$ ; \* $p = 0.036$ ; and  $>120$  cells/condition).  
(E) GFP-MPR-expressing cells treated as in (C) were analyzed by time-lapse microscopy (2 min, 0.5 s per frame). The number of TGN-derived tubules formed in one cell during 2 min were quantified ( $n = 3$ ; \*\* $p \leq 0.005$ ; and  $>80$  cells/condition). Data are shown as mean  $\pm$  SD (B, D, and E).  
(F–H) HeLa cells were co-transfected with CFP-FRB-Tgn38, mRFP-FKBP12-Sac1, or mRFP-FKBP12, and GFP-PH-FAPP1 (F), YFP-DBD (G), or GFP-CERT (H). After 1 day, cells were incubated with 1  $\mu$ M rapamycin for 20 min, then fixed, and analyzed by confocal microscopy. Fluorescence intensities along the lines are shown (right panels).  
(I–K) Fluorescence intensities in the TGN region and in the cytosol were measured for cells expressing GFP-PH-FAPP1 (I), YFP-DBD (J), or GFP-CERT (K), and the ratio TGN/cytosol was calculated ( $n = 3$  independent experiments in duplicate;  $>100$  cells/condition; median  $\pm$  SD; and \*\* $p < 0.001$ ). Scale bars, 10  $\mu$ m.

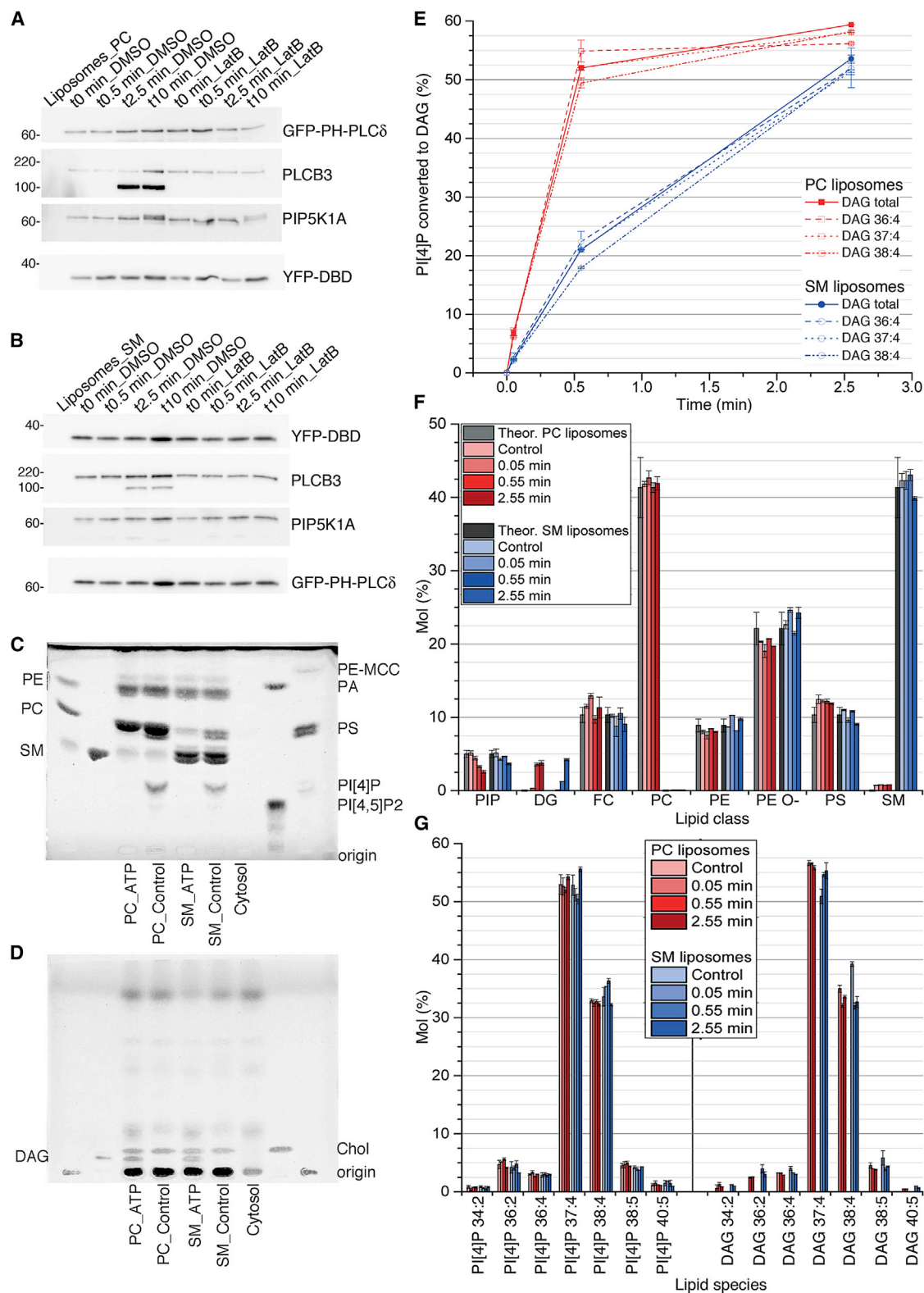


**Figure 4. PI[4]P to DAG Conversion on Synthetic Membranes**

(A and B) Liposomes containing the gE/gpI cd peptide, PI[4]P, and PC (A) or SM (B) were incubated with ATP, GTP $\gamma$ S, and cytosol of HEK cells expressing YFP-DBD or GFP-PLC $\delta$ -PH for the indicated times, in the presence of control DMSO or 20  $\mu$ M LatB. Proteins recruited onto liposomes were analyzed by western

(legend continued on next page)

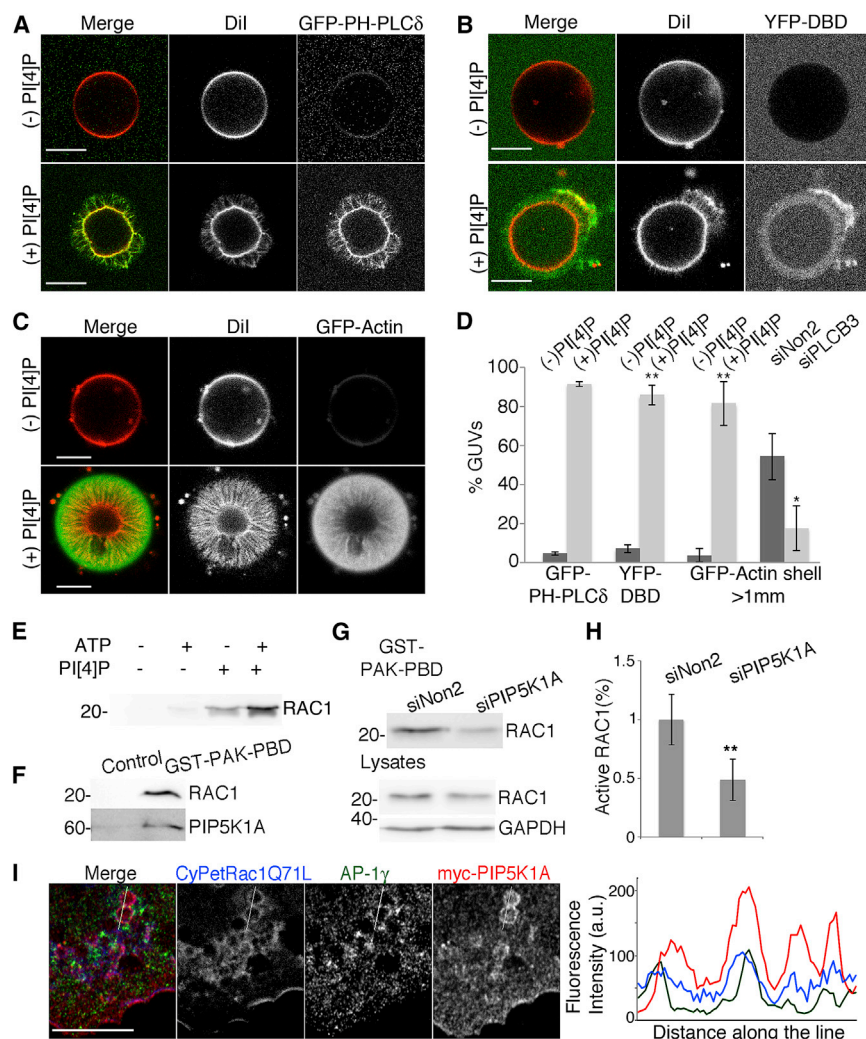


### Figure 5. DAG Production and Actin Polymerization during Clathrin/AP-1-Coated Carrier Biogenesis

(A–C) SM-containing GUVs with or without PI[4]P were incubated with GTP $\gamma$ S, ATP, and cytosol from HEK cells stably expressing GFP-PLC $\delta$ -PH (A), YFP-DBD (B), or GFP-actin (C) and analyzed by microscopy.

(D) The percentages of GUVs that recruited GFP-PLC $\delta$ -PH, YFP-DBD, or displayed GFP-actin tubules longer than 1  $\mu$ m are shown. In the last two conditions in the graph, GUVs containing PI[4]P were incubated with cytosol of GFP-actin-expressing cells treated with siNon2 or siPLCB3 (mean  $\pm$  SD; n = 3; \*\*p < 0.001; \*p < 0.02; and >25 GUVs/condition). GUVs were analyzed by confocal microscopy. Scale bars, 10  $\mu$ m.

(E) Liposomes containing gE/gpI cd peptide, SM, GTP $\gamma$ S,  $\pm$ ATP, or  $\pm$ PI[4]P, were incubated with HeLa cell cytosol for 15 min. RAC1 recruitment on liposomes was analyzed by western blot using anti-RAC1 antibodies.

(F and G) HeLa cells were treated with the indicated siRNAs for 72 hr. Active GTP-bound RAC1 was immunoprecipitated from the corresponding lysates of non-treated (F) or siRNAi-treated (G) cells using GST-PAK PBD beads or control glutathione Sepharose beads and analyzed by western blotting using antibodies against RAC1, PIP5K1A, and GAPDH in the immunoprecipitates (GST-PAK-PBD) and whole cell lysates (lysates). (H) The amount of active RAC1 levels by western blot (G) was quantified using ImageJ and normalized to total RAC1 and GAPDH (mean  $\pm$  SD; n = 4; and \*\*p < 0.001).

(I) HeLa cells co-transfected with CyPET-Rac1Q71L (blue) and myc-PIP5K1A were fixed and labeled with antibodies against AP-1 $\gamma$  (green) and myc (red). Fluorescence intensities along the lines are shown (right panels). Cells were analyzed by confocal microscopy. Scale bars, 10  $\mu$ m.

phosphatase 3 (PPAP2B) active at the Golgi-ER interface (Gutiérrez-Martínez et al., 2013). These various substrates may generate distinct DAG species with different biophysical properties. For example, it has been suggested that monounsaturated DAG species may be synthesized in the PLD/PA phosphohydrolase pathway, whereas polyunsaturated DAGs in the PI[4,5]P<sub>2</sub>/PLC pathway (Pessin and Raben, 1989; Pettitt et al., 1997).

The nature of the fatty acids in DAGs generated from different substrates may influence lipid packing, as suggested for ER-to-Golgi transport (Bigay and Antonny, 2012), and different DAGs may bind and recruit, with different affinities, specific proteins (Wakelam, 1998; Bigay and Antonny, 2012). In addition, DAGs synthesis and their segregation from PIPs may generate membrane nanodomains that recruit specific enzymes

blotting. YFP-DBD and GFP-PH-PLC $\delta$  were detected with an anti-GFP. The lower band observed for PLCB3 is a product of endogenous cleavage (Banno et al., 1995), n = 3. Data were quantified as shown in Figure S4A.

(C and D) Liposomes were incubated for 10 min with mouse brain cytosol, GTP $\gamma$ S, and an ATP regenerating system. Lipids were extracted and analyzed by thin-layer chromatography, using different mobile phases to separate polar lipids (including PI[4]P) (C) or non-polar lipids (including DAG) (D).

(E–G) The lipid composition of PC- or SM-containing liposomes (prepared as above) was determined by mass spectrometry.

(E) The percentages of PI converted to DAG on PC (red) or SM (blue) liposomes are shown. Average DAG conversion is illustrated with a solid line and a filled symbol; selected DAG species are shown with dash/dot lines and empty symbols. Data are shown as mean  $\pm$  SD between technical replicates.

(F) The lipid class composition of PC (red) and SM (blue) liposomes, as well as the theoretical compositions are shown (gray; mean  $\pm$  SD between technical replicates). The relative SD for the theoretical composition equals 10%. Mol% PE and PE O– was calculated based on theoretical quantity multiplied by experimental determined ratio.

(G) The molecular species profiles detected in the PI[4]P mixture and among the newly synthesized DAG are shown for both PC (red) and SM (blue) liposomes. DAGs were not detected in control samples. The different PI or DAG species were normalized to the total amount of the corresponding lipid class detected in the respective sample (mean  $\pm$  SD between technical replicates). Control, untreated liposomes; chol, free cholesterol.



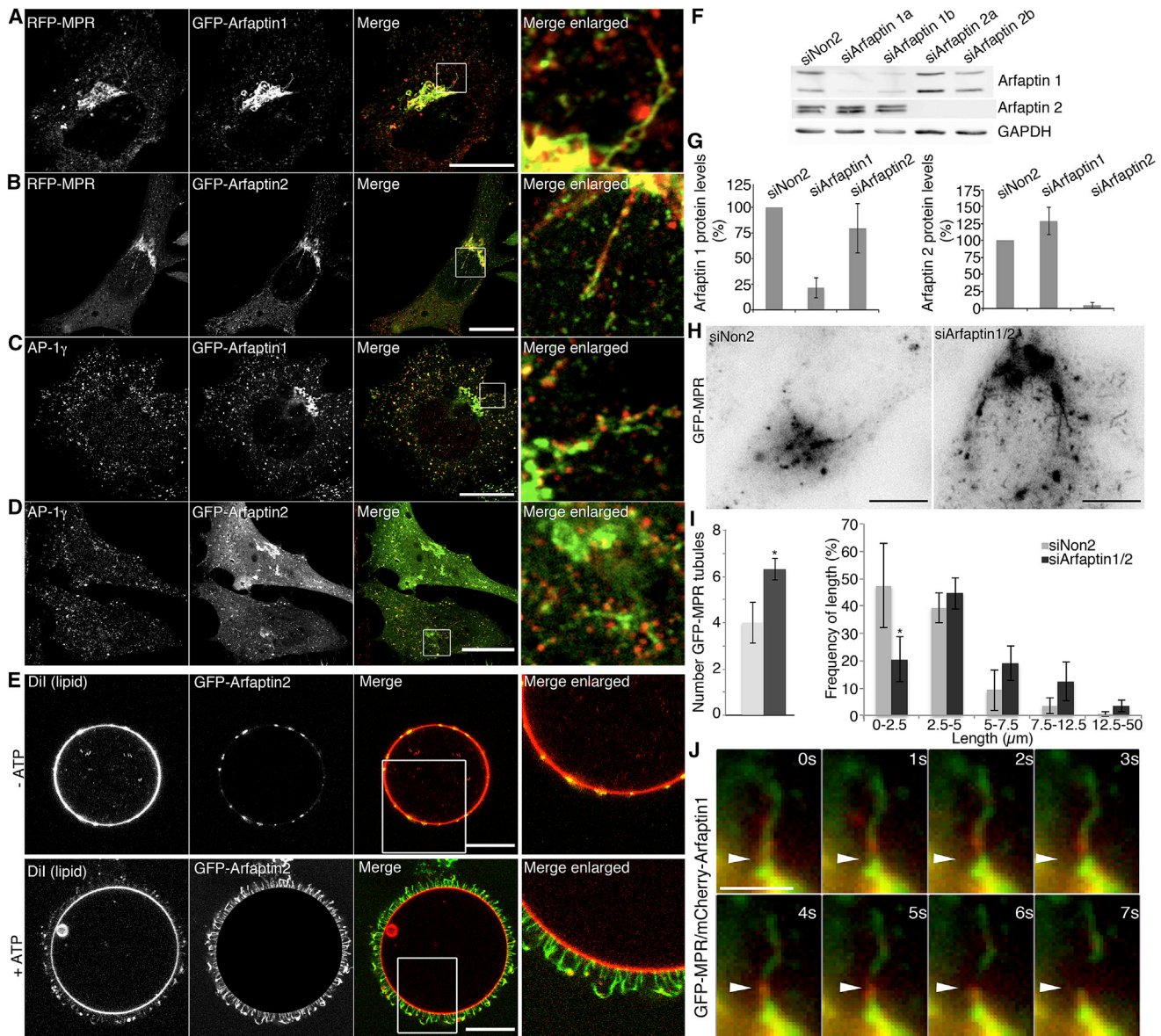


**Figure 6. Arfaptin-1 and -2 Guide Membrane Scission**

(A–D) HeLa cells expressing RFP-CIMPR (red) and GFP-arfaptin-1 (A) or GFP-arfaptin-2 (B), or GFP-arfaptin-1 (C), or GFP-arfaptin-2 (D) and co-labeled with anti-AP-1 $\gamma$  were analyzed by confocal fluorescence microscopy. The right panels illustrate details of tubular structures in the Golgi region.

(E) GUVs containing gE/gpl cd peptide, PI[4]P, and the lipid dye Dil (red) were incubated with GTP $\gamma$ S and cytosol from HEK cells stably expressing GFP-arfaptin-2, with or without ATP.

(F–I) GFP-MPR cells were treated for 72 hr with siNon2, or siRNAs targeting arfaptin-1 and/or arfaptin-2.

(F and G) The knockdown efficiencies were evaluated by western blotting using indicated antibodies (F) and quantified (G) (mean  $\pm$  SD; n = 3). Note that both arfaptin-1 isoforms are depleted by siArfaptin-1.

(H) GFP-MPR dynamics in cells depleted of both arfaptin-1 and arfaptin-2 were analyzed by live cell imaging (2 min, 0.5 s per frame). Representative images are shown for each condition (inverted images presented, see Movie S5).

(I) The number and the length of the TGN-derived GFP-MPR<sup>+</sup> tubules formed during 2 min in one cell were quantified (mean  $\pm$  SD; n = 3; \*p < 0.03; and  $\geq$  85 cells/condition).

(J) HeLa cells expressing GFP-MPR and mCherry-arfaptin-1 were analyzed by time-lapse microscopy (2 min, 1 s per frame). Representative frames are depicted. The arrowheads indicate arfaptin-1 recruitment followed by a fission event. Scale bars, 10  $\mu$ m (A–C), 8  $\mu$ m (F), 10  $\mu$ m (I), and 2.5  $\mu$ m (K).

(Ahyayauch et al., 2015), such as curvature generators or signaling molecules. For example, recent data indicate that an increase in DAG levels on Golgi membranes, through activation

of PKD-dependent signaling, leads to depletion of PI[4]P and PI[4]P-binding proteins (Capasso et al., 2017). Last, but not least, the conversion of cylindrical, negatively charged, PIPs to conical,

neutral DAGs modifies the biophysical characteristics of membranes (Kozlov et al., 2014).

These changes in the biochemical and biophysical properties of lipid bilayers may sustain the mechanical forces generated by actin polymerization and actin-based motors (Anitei and Hoflack, 2011) needed to overcome membrane rigidity and change membrane shape.

How are the chemical/biophysical properties of membranes and actin-based mechanical forces coordinated to change membrane shape? ARF-1-dependent clathrin/AP-1 coat assembly controls actin polymerization due to interactions between the clathrin heavy chain and CYFIP1/2, a component of the nucleation promoting complex WAVE, that binds RAC1 (Anitei et al., 2010). The activities of the ARF1 and RAC1 are coupled through a complex comprising the GIT1/2 ARF1 GTPase-activating proteins and the  $\beta$ -PIX RAC1 exchange factor (Baust et al., 2006). Activated RAC1 may recruit onto membranes PIP5K1A, an enzyme needed for DAG production and actin polymerization. Thus, clathrin/AP-1 coat assembly, by controlling RAC1 activation, would synchronize membrane lipid modifications and actin polymerization to change membrane shape. These changes may power the subsequent steps in carrier biogenesis; e.g., scission.

The BAR-domain-containing arfaptins-1/2 are recruited onto tubular membranes. They are not essential for the biogenesis of clathrin/AP-1-coated tubules, but guide their scission, as also seen for immature secretory granules (Gehart et al., 2012). How do arfaptins control scission? First, they may recruit proteins involved in scission, such as PLD, PKD, or ARF1 dimers, as seen on COPI-coated membranes (Beck et al., 2011; Shin and Exton, 2005; Williger et al., 1999). Second, arfaptins, by covering lipid domains, may stabilize them and cause lipid segregation (Zhao et al., 2013). Arfaptins may restrict the membrane accessibility of proteins that function in scission (Liu et al., 2006). Although we detected dynamin isoforms on tubular membranes, so far we, and others (Kural et al., 2012), could not show their implication in clathrin/AP-1 carrier scission. Lipid segregation between arfaptin covered and uncovered areas could increase line tension between arfaptin-positive and -negative domains, leading to scission, as described for endocytosis (Johannes and Mayor, 2010; Römer et al., 2010). A recent study argues for this latter hypothesis, demonstrating that, in vitro, a BAR domain protein scaffold creates a frictional barrier for lipid diffusion (Simunovic et al., 2017). During molecular-motor-dependent membrane elongation, this friction between the protein scaffold and the underlying membrane contributes to scission. The next challenge will be to understand how the chemical and biophysical properties of membrane domains and arfaptins contribute to this process.

## EXPERIMENTAL PROCEDURES

### Cell Culture

Cells were grown at 37°C and 5% CO<sub>2</sub> in DMEM + GlutaMAX (4.5 mg/mL glucose, containing pyruvate), supplemented with penicillin/streptomycin, 2 mM L-glutamine and 10% (v/v) fetal bovine serum superior (Biochrom, Germany). For transient transfection, 24 hr after seeding, cells were incubated with the indicated DNA constructs and jetPEI reagent (Polyplus-transfection, France) or the indicated siRNAs and INTERFERin (Polyplus-transfection), according to supplier's protocols. Cell lines were obtained as described in Supplemental Experimental Procedures.

### Protein Recruitment onto Liposomes and Mass-Spectrometry-Based Proteomic Analysis

Protein recruitment onto liposomes and mass spectrometry-based proteomic analysis were performed as in Baust et al. (2006) and Niehage et al. (2014). Liposomes were made of a mixture of lipids containing PC (1,2-dioleoyl-sn-glycero-3-phosphocholine), SM (porcine brain extract), PE (porcine brain extract), PS (porcine brain extract), cholesterol (free cholesterol), maleimide lipid anchor (18:1 1,2-dioleoyl-sn-glycero-3-phosphoethanolamine-N-[4-(p-maleimidomethyl)cyclohexane-carboxamide [PE-MCC]], and PI[4]P (porcine brain extract) or (when indicated) PI[4,5]P2 (porcine brain extract) in a molar ratio of 41.5%: 31.5%: 10.5%: 10.5%: 1%: 5%. For GUV formation, DiI-C16 was added in a molar ratio of 0.02%. Liposomes were coupled to the gE/gpI cd peptide (NH<sub>2</sub>-CGKRMRVKAYRVKSPYNQSMYYAGLPVDD-FEDESTDTEE-COOH) synthesized by EZBiolab (IN, USA) or produced as described in Niehage et al. (2014). Cytosolic extract (protein concentration 4 mg/mL) was supplemented with 100  $\mu$ M GTP $\gamma$ S, and, when indicated, an ATP-regeneration system (1 mM ATP, 10 mM creatine phosphate, and 10  $\mu$ g/mL creatine kinase), and 20  $\mu$ M latrunculin B. Liposomes were added to a final concentration of about 200 nmol/mL. The mixture was incubated at 37°C for indicated times. Reaction was stopped by the addition of 1 mL of cold recruitment buffer. Liposomes were separated from the cytosol mixture by centrifugation (20,000 g for 15 min). Pellets were resuspended in 25  $\mu$ L of 2 $\times$  Laemmli buffer and analyzed by SDS-PAGE and western blot or mass spectrometry-based proteomic analysis. GUVs were prepared and analyzed by microscopy as in Anitei et al. (2010) and Bacia et al. (2004). All mass spectrometry data will be made available upon request.

### Thin Layer Chromatography and Mass-Spectrometry-Based Lipidomics

Lipids were extracted immediately after liposome incubation with cytosol, and analyzed either by thin layer chromatography (TLC) or by shotgun lipidomics. All mass spectrometry data will be made available upon request.

### Microscopy

Fixed samples were imaged using a LSM700 or a LSM780 microscope. High-speed time-lapse microscopy was performed with an AFLX6000 microscope equipped with an electron multiplying charge-coupled device (EMCCD) detector, with an Axiovert 200 M microscope (Carl Zeiss), or using spinning disk microscopy (Nikon, Japan, PICT-IBISA Imaging Facility, Paris, France).

### RAC1 Activation Assay

Active RAC1 was immunoprecipitated from cell lysates using PAK-GST beads (1 mg/mL, Cytoskeleton Inc., CO, USA) and analyzed by SDS-PAGE and western blot. More details on each method are described in Supplemental Experimental Procedures.

## SUPPLEMENTAL INFORMATION

Supplemental Information includes Supplemental Experimental Procedures, five figures, two tables, and five movies and can be found with this article online at <http://dx.doi.org/10.1016/j.celrep.2017.08.013>.

## AUTHOR CONTRIBUTIONS

M.A. and C.S. designed, performed, and analyzed the experiments. C.C. and C.N. performed and analyzed the mass spectrometry experiments. K.S. and A.S. performed the MS lipid analysis. A.C., P.S., and U.C. performed the TLC lipid analysis. T.P. contributed to the cell and molecular biology experiments. B.H. designed and analyzed experiments and wrote the manuscript with C.S. and M.A.

## ACKNOWLEDGMENTS

We thank lab members for their helpful discussions and critical comments. We thank Tamas Balla (NIH/NICHD, Massachusetts) and Neale Ridgway (Canada) for DNA constructs. We thank Dr. Eberhard Krause (FMP, Berlin, Germany) for



providing the LTQ Orbitrap XL mass spectrometer. We also thank Dr. Jean Salamero (Curie Institute, Paris France) for providing the access to the Euro-Bio-imaging Facility. The research of B.H. was supported in part by grants from DFG (TRR 83/1-2010, HO 2584/1-1, HO 2584/2-1, HO 2584/6-1, HO 2584/8-1, and HO 2584/9-1) and TU-Dresden (Program Support the Best). The research of B.H., A.S., and U.C. was supported in part by TRR 83/1-2014.

Received: May 3, 2017

Revised: June 29, 2017

Accepted: July 31, 2017

Published: August 29, 2017

## REFERENCES

- Ahyayauch, H., Sot, J., Collado, M.I., Huarte, N., Requejo-Isidro, J., Alonso, A., and Gofí, F.M. (2015). End-product diacylglycerol enhances the activity of PI-PLC through changes in membrane domain structure. *Biophys. J.* **108**, 1672–1682.
- Anitei, M., and Hoflack, B. (2011). Bridging membrane and cytoskeleton dynamics in the secretory and endocytic pathways. *Nat. Cell Biol.* **14**, 11–19.
- Anitei, M., Stange, C., Parshina, I., Baust, T., Schenck, A., Raposo, G., Kirchhausen, T., and Hoflack, B. (2010). Protein complexes containing CYFIP/Sra/PIR121 coordinate Arf1 and Rac1 signalling during clathrin-AP-1-coated carrier biogenesis at the TGN. *Nat. Cell Biol.* **12**, 330–340.
- Anitei, M., Chenna, R., Czupalla, C., Esner, M., Christ, S., Lenhard, S., Korn, K., Meyenhofer, F., Bickle, M., Zerial, M., and Hoflack, B. (2014). A high-throughput siRNA screen identifies genes that regulate mannose 6-phosphate receptor trafficking. *J. Cell Sci.* **127**, 5079–5092.
- Bacia, K., Scherfeld, D., Kahya, N., and Schwille, P. (2004). Fluorescence correlation spectroscopy relates rafts in model and native membranes. *Biophys. J.* **87**, 1034–1043.
- Banno, Y., Nakashima, S., Hachiya, T., and Nozawa, Y. (1995). Endogenous cleavage of phospholipase C- $\beta$  3 by agonist-induced activation of calpain in human platelets. *J. Biol. Chem.* **270**, 4318–4324.
- Baron, C.L., and Malhotra, V. (2002). Role of diacylglycerol in PKD recruitment to the TGN and protein transport to the plasma membrane. *Science* **295**, 325–328.
- Baust, T., Czupalla, C., Krause, E., Bourel-Bonnet, L., and Hoflack, B. (2006). Proteomic analysis of adaptor protein 1A coats selectively assembled on liposomes. *Proc. Natl. Acad. Sci. USA* **103**, 3159–3164.
- Beck, R., Prinz, S., Diestelkötter-Bachert, P., Röhling, S., Adolf, F., Hoehner, K., Welsch, S., Ronchi, P., Brügger, B., Briggs, J.A., and Wieland, F. (2011). Coatamer and dimeric ADP ribosylation factor 1 promote distinct steps in membrane scission. *J. Cell Biol.* **194**, 765–777.
- Bigay, J., and Antonny, B. (2012). Curvature, lipid packing, and electrostatics of membrane organelles: defining cellular territories in determining specificity. *Dev. Cell* **23**, 886–895.
- Brown, H.A., Gutowski, S., Moomaw, C.R., Slaughter, C., and Sternweis, P.C. (1993). ADP-ribosylation factor, a small GTP-dependent regulatory protein, stimulates phospholipase D activity. *Cell* **75**, 1137–1144.
- Capasso, S., Sticco, L., Rizzo, R., Pirozzi, M., Russo, D., Dathan, N.A., Campelo, F., van Galen, J., Hölttä-Vuori, M., Turacchio, G., et al. (2017). Sphingolipid metabolic flow controls phosphoinositide turnover at the trans-Golgi network. *EMBO J.* **36**, 1716–1754.
- Chao, W.T., Daquinag, A.C., Ashcroft, F., and Kunz, J. (2010). Type I PIPK- $\alpha$  regulates directed cell migration by modulating Rac1 plasma membrane targeting and activation. *J. Cell Biol.* **190**, 247–262.
- Cruz-Garcia, D., Ortega-Bellido, M., Scarpa, M., Villeneuve, J., Jovic, M., Porzner, M., Balla, T., Seufferlein, T., and Malhotra, V. (2013). Recruitment of arfaptins to the trans-Golgi network by PI(4)P and their involvement in cargo export. *EMBO J.* **32**, 1717–1729.
- Di Paolo, G., and De Camilli, P. (2006). Phosphoinositides in cell regulation and membrane dynamics. *Nature* **443**, 651–657.
- Díaz Añel, A.M. (2007). Phospholipase C  $\beta$ 3 is a key component in the Gbetagamma/PKC $\zeta$ /PKD-mediated regulation of trans-Golgi network to plasma membrane transport. *Biochem. J.* **406**, 157–165.
- Doray, B., Ghosh, P., Griffith, J., Geuze, H.J., and Kornfeld, S. (2002). Cooperation of GGAs and AP-1 in packaging MPRs at the trans-Golgi network. *Science* **297**, 1700–1703.
- Fugmann, T., Hausser, A., Schöffler, P., Schmid, S., Pfizenmaier, K., and Olayioye, M.A. (2007). Regulation of secretory transport by protein kinase D-mediated phosphorylation of the ceramide transfer protein. *J. Cell Biol.* **178**, 15–22.
- Gallegos, L.L., Kunkel, M.T., and Newton, A.C. (2006). Targeting protein kinase C activity reporter to discrete intracellular regions reveals spatiotemporal differences in agonist-dependent signaling. *J. Biol. Chem.* **281**, 30947–30956.
- Gehart, H., Goginashvili, A., Beck, R., Morvan, J., Erbs, E., Formentini, I., De Matteis, M.A., Schwab, Y., Wieland, F.T., and Ricci, R. (2012). The BAR domain protein Arfaptin-1 controls secretory granule biogenesis at the trans-Golgi network. *Dev. Cell* **23**, 756–768.
- Ghosh, P., Dahms, N.M., and Kornfeld, S. (2003). Mannose 6-phosphate receptors: new twists in the tale. *Nat. Rev. Mol. Cell Biol.* **4**, 202–212.
- Godi, A., Pertile, P., Meyers, R., Marra, P., Di Tullio, G., Iurisci, C., Luini, A., Corda, D., and De Matteis, M.A. (1999). ARF mediates recruitment of PtdIns-4-OH kinase- $\beta$  and stimulates synthesis of PtdIns(4,5)P<sub>2</sub> on the Golgi complex. *Nat. Cell Biol.* **1**, 280–287.
- Gutiérrez-Martínez, E., Fernández-Ulibarri, I., Lázaro-Diéguez, F., Johannes, L., Pyne, S., Sarri, E., and Egea, G. (2013). Lipid phosphate phosphatase 3 participates in transport carrier formation and protein trafficking in the early secretory pathway. *J. Cell Sci.* **126**, 2641–2655.
- Hanada, K., Kumagai, K., Tomishige, N., and Yamaji, T. (2009). CERT-mediated trafficking of ceramide. *Biochim. Biophys. Acta* **1791**, 684–691.
- Haucke, V., and Di Paolo, G. (2007). Lipids and lipid modifications in the regulation of membrane traffic. *Curr. Opin. Cell Biol.* **19**, 426–435.
- Huitema, K., van den Dikkenberg, J., Brouwers, J.F., and Holthuis, J.C. (2004). Identification of a family of animal sphingomyelin synthases. *EMBO J.* **23**, 33–44.
- Johannes, L., and Mayor, S. (2010). Induced domain formation in endocytic invagination, lipid sorting, and scission. *Cell* **142**, 507–510.
- Kaksonen, M., Toret, C.P., and Drubin, D.G. (2006). Harnessing actin dynamics for clathrin-mediated endocytosis. *Nat. Rev. Mol. Cell Biol.* **7**, 404–414.
- Kanoh, H., Williger, B.T., and Exton, J.H. (1997). Arfaptin 1, a putative cytosolic target protein of ADP-ribosylation factor, is recruited to Golgi membranes. *J. Biol. Chem.* **272**, 5421–5429.
- Kozlov, M.M., Campelo, F., Liska, N., Chernomordik, L.V., Marrink, S.J., and McMahon, H.T. (2014). Mechanisms shaping cell membranes. *Curr. Opin. Cell Biol.* **29**, 53–60.
- Kural, C., Tacheva-Grigoriou, S.K., Boulant, S., Cocucci, E., Baust, T., Duarte, D., and Kirchhausen, T. (2012). Dynamics of intracellular clathrin/AP1- and clathrin/AP3-containing carriers. *Cell Rep.* **2**, 1111–1119.
- Le Borgne, R. (2006). Regulation of Notch signalling by endocytosis and endosomal sorting. *Curr. Opin. Cell Biol.* **18**, 213–222.
- Le Borgne, R., and Hoflack, B. (1998). Mechanisms of protein sorting and coat assembly: insights from the clathrin-coated vesicle pathway. *Curr. Opin. Cell Biol.* **10**, 499–503.
- Legendre-Guillemin, V., Wasiak, S., Hussain, N.K., Angers, A., and McPherson, P.S. (2004). ENTH/ANTH proteins and clathrin-mediated membrane budding. *J. Cell Sci.* **117**, 9–18.
- Liu, J., Kaksonen, M., Drubin, D.G., and Oster, G. (2006). Endocytic vesicle scission by lipid phase boundary forces. *Proc. Natl. Acad. Sci. USA* **103**, 10277–10282.
- Lundmark, R., Doherty, G.J., Vallis, Y., Peter, B.J., and McMahon, H.T. (2008). Arf family GTP loading is activated by, and generates, positive membrane curvature. *Biochem. J.* **414**, 189–194.

- Man, Z., Kondo, Y., Koga, H., Umino, H., Nakayama, K., and Shin, H.W. (2011). Arfaptins are localized to the trans-Golgi by interaction with Arl1, but not Arfs. *J. Biol. Chem.* **286**, 11569–11578.
- Méresse, S., and Hoflack, B. (1993). Phosphorylation of the cation-independent mannose 6-phosphate receptor is closely associated with its exit from the trans-Golgi network. *J. Cell Biol.* **120**, 67–75.
- Méresse, S., Ludwig, T., Frank, R., and Hoflack, B. (1990). Phosphorylation of the cytoplasmic domain of the bovine cation-independent mannose 6-phosphate receptor. Serines 2421 and 2492 are the targets of a casein kinase II associated to the Golgi-derived HAI adaptor complex. *J. Biol. Chem.* **265**, 18833–18842.
- Mootha, V.K., Lindgren, C.M., Eriksson, K.F., Subramanian, A., Sihag, S., Lehar, J., Puigserver, P., Carlsson, E., Ridderstråle, M., Laurila, E., et al. (2003). PGC-1 $\alpha$ -responsive genes involved in oxidative phosphorylation are coordinately downregulated in human diabetes. *Nat. Genet.* **34**, 267–273.
- Niehage, C., Stange, C., Anitei, M., and Hoflack, B. (2014). Liposome-based assays to study membrane-associated protein networks. *Methods Enzymol.* **534**, 223–243.
- Pessin, M.S., and Raben, D.M. (1989). Molecular species analysis of 1,2-diglycerides stimulated by alpha-thrombin in cultured fibroblasts. *J. Biol. Chem.* **264**, 8729–8738.
- Pettitt, T.R., Martin, A., Horton, T., Liossis, C., Lord, J.M., and Wakelam, M.J. (1997). Diacylglycerol and phosphatidate generated by phospholipases C and D, respectively, have distinct fatty acid compositions and functions. Phospholipase D-derived diacylglycerol does not activate protein kinase C in porcine aortic endothelial cells. *J. Biol. Chem.* **272**, 17354–17359.
- Posor, Y., Eichhorn-Gruenig, M., Puchkov, D., Schöneberg, J., Ullrich, A., Lampe, A., Müller, R., Zerbakhsh, S., Gulluni, F., Hirsch, E., et al. (2013). Spatiotemporal control of endocytosis by phosphatidylinositol-3,4-bisphosphate. *Nature* **499**, 233–237.
- Qualmann, B., Koch, D., and Kessels, M.M. (2011). Let's go bananas: revisiting the endocytic BAR code. *EMBO J.* **30**, 3501–3515.
- Römer, W., Pontani, L.L., Sorre, B., Rentero, C., Berland, L., Chambon, V., Lamaze, C., Bassereau, P., Sykes, C., Gaus, K., and Johannes, L. (2010). Actin dynamics drive membrane reorganization and scission in clathrin-independent endocytosis. *Cell* **140**, 540–553.
- Schmidt, J.A., and Brown, W.J. (2009). Lysophosphatidic acid acyltransferase 3 regulates Golgi complex structure and function. *J. Cell Biol.* **186**, 211–218.
- Sciorra, V.A., Rudge, S.A., Prestwich, G.D., Frohman, M.A., Engebrecht, J., and Morris, A.J. (1999). Identification of a phosphoinositide binding motif that mediates activation of mammalian and yeast phospholipase D isoenzymes. *EMBO J.* **18**, 5911–5921.
- Shin, O.H., and Exton, J.H. (2001). Differential binding of arfaptin 2/POR1 to ADP-ribosylation factors and Rac1. *Biochem. Biophys. Res. Commun.* **285**, 1267–1273.
- Shin, O.H., and Exton, J.H. (2005). Assays and properties of arfaptin 2 binding to Rac1 and ADP-ribosylation factors (Arfs). *Methods Enzymol.* **404**, 359–367.
- Sicart, A., Katan, M., Egea, G., and Sarri, E. (2014). PLCgamma1 participates in protein transport and diacylglycerol production triggered by cargo arrival at the Golgi. *Traffic* **16**, 250–266.
- Simunovic, M., Manneville, J.B., Renard, H.F., Evergren, E., Raghunathan, K., Bhatia, D., Kenworthy, A.K., Voth, G.A., Prost, J., McMahon, H.T., et al. (2017). Friction mediates scission of tubular membranes scaffolded by BAR proteins. *Cell* **170**, 172–184.e11.
- Smyth, S.S., Sciorra, V.A., Sigal, Y.J., Pamuklar, Z., Wang, Z., Xu, Y., Prestwich, G.D., and Morris, A.J. (2003). Lipid phosphate phosphatases regulate lysophosphatidic acid production and signaling in platelets: studies using chemical inhibitors of lipid phosphate phosphatase activity. *J. Biol. Chem.* **278**, 43214–43223.
- Stauffer, T.P., Ahn, S., and Meyer, T. (1998). Receptor-induced transient reduction in plasma membrane PtdIns(4,5)P<sub>2</sub> concentration monitored in living cells. *Curr. Biol.* **8**, 343–346.
- Subramanian, A., Tamayo, P., Mootha, V.K., Mukherjee, S., Ebert, B.L., Gillette, M.A., Paulovich, A., Pomeroy, S.L., Golub, T.R., Lander, E.S., and Mesirov, J.P. (2005). Gene set enrichment analysis: a knowledge-based approach for interpreting genome-wide expression profiles. *Proc. Natl. Acad. Sci. USA* **102**, 15545–15550.
- Szentpetery, Z., Várnai, P., and Balla, T. (2010). Acute manipulation of Golgi phosphoinositides to assess their importance in cellular trafficking and signaling. *Proc. Natl. Acad. Sci. USA* **107**, 8225–8230.
- Tolias, K.F., Hartwig, J.H., Ishihara, H., Shibasaki, Y., Cantley, L.C., and Carpenter, C.L. (2000). Type I $\alpha$  phosphatidylinositol-4-phosphate 5-kinase mediates Rac-dependent actin assembly. *Curr. Biol.* **10**, 153–156.
- Traub, L.M., and Bonifacio, J.S. (2013). Cargo recognition in clathrin-mediated endocytosis. *Cold Spring Harb. Perspect. Biol.* **5**, a016790.
- Waguri, S., Dewitte, F., Le Borgne, R., Rouillé, Y., Uchiyama, Y., Dubremetz, J.F., and Hoflack, B. (2003). Visualization of TGN to endosome trafficking through fluorescently labeled MPR and AP-1 in living cells. *Mol. Biol. Cell* **14**, 142–155.
- Wakelam, M.J. (1998). Diacylglycerol—when is it an intracellular messenger? *Biochim. Biophys. Acta* **1436**, 117–126.
- Wang, E., Norred, W.P., Bacon, C.W., Riley, R.T., and Merrill, A.H., Jr. (1991). Inhibition of sphingolipid biosynthesis by fumonisins. Implications for diseases associated with *Fusarium moniliforme*. *J. Biol. Chem.* **266**, 14486–14490.
- Wang, Y.J., Wang, J., Sun, H.Q., Martinez, M., Sun, Y.X., Macia, E., Kirchhausen, T., Albanesi, J.P., Roth, M.G., and Yin, H.L. (2003). Phosphatidylinositol 4 phosphate regulates targeting of clathrin adaptor AP-1 complexes to the Golgi. *Cell* **114**, 299–310.
- Williger, B.T., Provost, J.J., Ho, W.T., Milstine, J., and Exton, J.H. (1999). Arfaptin 1 forms a complex with ADP-ribosylation factor and inhibits phospholipase D. *FEBS Lett.* **454**, 85–89.
- Yang, J.S., Gad, H., Lee, S.Y., Mironov, A., Zhang, L., Beznoussenko, G.V., Valente, C., Turacchio, G., Bonsra, A.N., Du, G., et al. (2008). A role for phosphatidic acid in COPI vesicle fission yields insights into Golgi maintenance. *Nat. Cell Biol.* **10**, 1146–1153.
- Yang, Q., Zhang, X.F., Van Goor, D., Dunn, A.P., Hyland, C., Medeiros, N., and Forscher, P. (2013). Protein kinase C activation decreases peripheral actin network density and increases central nonmuscle myosin II contractility in neuronal growth cones. *Mol. Biol. Cell* **24**, 3097–3114.
- Zhao, H., Michelot, A., Koskela, E.V., Tkach, V., Stamou, D., Drubin, D.G., and Lappalainen, P. (2013). Membrane-sculpting BAR domains generate stable lipid microdomains. *Cell Rep.* **4**, 1213–1223.

**Supplemental Information**

**Spatiotemporal Control of Lipid Conversion, Actin-  
Based Mechanical Forces, and Curvature Sensors  
during Clathrin/AP-1-Coated Vesicle Biogenesis**

**Mihaela Anitei, Christoph Stange, Cornelia Czupalla, Christian Niehage, Kai Schuhmann, Pia Sala, Aleksander Czogalla, Theresia Pursche, Ünal Coskun, Andrej Shevchenko, and Bernard Hoflack**

## SUPPLEMENTAL DATA

### SUPPLEMENTAL EXPERIMENTAL PROCEDURES

**Reagents:** GTP $\gamma$ S (Guanosine 5'-O-(3-Thiotriphosphate)), ATP, creatine phosphokinase, creatine phosphate and complete protease inhibitors were from Roche Diagnostics, Germany. Inhibitors: latrunculin B (Calbiochem/Merck, Germany), fumonisin B1 (Cayman Chemical, MI, USA), phorbol 12,13-dibutyrate (PDBu) (Sigma-Aldrich, Germany), and rapamycin (LC laboratories, MA, USA). Fluorescent Alexa-fluorophore labeled secondary antibodies, DAPI and DiI-C16 were from Molecular Probes/Life Technologies (Germany). HRP-conjugated secondary antibodies were from Dianova, Germany. Primary antibodies: mouse anti-arfaptin-2 (clone 2B5) (Sigma-Aldrich); goat anti-arfaptin-1 (I-19) and rabbit anti-PLCB3 (C20) (Santa Cruz Biotechnology, TX, USA); rabbit anti-PIP5K1A (15713-1-AP, Proteintech Group, IL, USA); mouse anti-AP-1- $\gamma$  (clone 88), anti-GM130, anti-RAC1 and anti-tubulin b (BD Biosciences, CA, USA), rabbit anti-p34-Arc/ARPC2 (Millipore), mouse anti-GAPDH (Acris Antibodies, Germany), rabbit anti-clathrin heavy chain (ab21679, Abcam, UK), rabbit anti-PPAP2A and rabbit anti-PLD1 (EP1506Y) (GeneTex, CA, USA), mouse IgM anti-GTP-RAC1 (New East Biosciences, PA, USA), sheep anti-TGN46 (Novus Biologicals, CO, USA), mouse IgM anti-PI[4,5]P2 (Echelon Biosciences, UT, USA), anti-GFP clone 7.1 and 13.1 (Roche Life Science, Germany), mouse anti-human transferrin receptor (clone H68.4) (Zymed, Life Technologies).

**DNA constructs:** The mammalian expression vectors pEGFP-N3, pEGFP-C1, and pmCherry-C1 were from Takara Bio Europe/Clontech (France). Plasmids used: YFP-DBD (Addgene plasmid 14874)(Gallegos et al., 2006); GFP-PLC $\delta$ -PH (Addgene plasmid 21179)(Stauffer et al., 1998), GFP-CERT(Kawano et al., 2006), GFP-PH-FAPP1(Balla et al., 2005), mRFP-FKBP12-hSac1, mRFP-FKBP12 and CFP-Tgn38-FRP(Szentpetery et al., 2010), pEGFP-ciMPR, mCherry-ciMPR and pmRFP-ciMPR(Waguri et al., 2003), GFP-actin (BD Bioscience, CA, USA), myc-PIP5K1A(Rozelle et al., 2000), HA-Rac1V12 (Tobias Heckel, Roche Diagnostics, Switzerland), pCyPet RAC1Q71L- (Addgene plasmid 22783)(Machacek et al., 2009).

The coding sequence of human arfaptin-1 was amplified from HeLa cell cDNA and its large splice variant (373 aa) was cloned into pEGFP-C1 and into pmCherry-C1. The coding sequence of human arfaptin-2 was amplified from HeLa cell cDNA and was cloned into pGFP-N3.

**Cell lines and transfection:** HeLa and HEK-293T cell lines were from the American Type Culture Collection (LGC Standards GmbH, Germany). GFP-MPR expressing HeLa cells were described in(Waguri et al., 2003). BSC-1 cells stably expressing GFP-AP-1- $\sigma$  were a gift from Tomas Kirchhausen (Harvard Medical School, MA, USA). HEK cells stably expressing GFP-arfaptin-2, GFP-actin, YFP-DBD or GFP-PLC $\delta$ -PH were generated as described below. Cells grown in one well of a 24-well plate were transfected with 1  $\mu$ g plasmid DNA. Two days after transfection, cells were detached with trypsin and seeded into 10 cm dishes containing medium supplemented with 0.8 mg/ml Geneticin (Gibco, Life Technologies). After 2-3 weeks, single clone-derived colonies were picked and transferred into wells of a 24-well plate. Clones were individually analyzed for expression by fluorescence microscopy and/or Western blot, and suitable clones were grown with 0.3 mg/ml Geneticin. All cell culture reagents were purchased from Gibco/Life Technologies.

**RNA interference:** All small interfering RNAs (siRNAs) were supplied as annealed Silencer Select Pre-Designed siRNAs (Ambion//Life Technologies) or stealth siRNA (Invitrogen/Life Technologies) and were stored at -20° C, as 20  $\mu$ M stock solutions in water.

siRNA sequences:

siArfaptin-1a (Entrez GeneID: 27236; 5'-GAAAUCCAGUGACUAGUAtt-3');  
siArfaptin-1b (Entrez GeneID: 27236; 5'-GGGUGUUAUUGAAGCAGGAtt-3');  
siArfaptin-2a (Entrez GeneID: 23647; 5'-GGACCCAACCUCAAUGAAAtt-3');  
siArfaptin-2b (Entrez GeneID: 23647; 5'-CAACUGUUAUCAGAACGAUtt-3');  
siPIP5K1A\_1 (Entrez GeneID: 8394; 5'-CAAGAUCGGUAAAAAUGCtt-3');  
stealth siPIP5K1A\_2 (5'-GCGUUCACCUUGGUCGUCCUGAUGU);  
siPLCB3\_1 (Entrez GeneID: 5331; 5'-GCAUAACACCUAUCUCACUtt-3');  
stealth siPLCB3\_2 (5'-GGCUUCACUUCGCAU UGCAGCCUUU-3');  
stealth siPLD1 (Entrez GeneID: 5337, 5'-CCAACUUUCUCAAAGAUCGAUU-3');  
stealth siPLD2 (5'-CAGGUGGUGGGC ACCGAAAGAUUA-3');  
stealth siPPAP2A (Entrez GeneID: 8611, 5'-UAGUAUUCAAUGUAACCAUCGCUGC-3').

siNon2 represents Silencer Select Negative Control #2 (Ambion/Life Technologies). The siRNAs were delivered into cells at a final concentration of 10 nM (24 or 6 well plates) or 20 nM (10 cm plates), using INTERFERIN reagent (Polyplus Transfection, France) according to supplier's protocol. Cells were treated with siRNAs for 72 h prior to analysis.

**Cytosol preparation.** Mouse brains (female CD1, Biomedical Service Unit of the MPI-CBG, Dresden, Germany) were dissected, the cerebellum and the meninges were removed, and the remaining brain tissue was homogenized, using a dounce tissue grinder (Wheaton Science Products, NJ, USA), in 3 volumes of homogenization buffer (25 mM HEPES, pH 7.2, 125 mM potassium acetate, 2.5 mM magnesium acetate, supplemented with 2 mM Na<sub>2</sub>V<sub>2</sub>O<sub>4</sub>, 5 mM NaF, 50 mM beta-glycerol phosphate and complete protease inhibitor mix). The homogenate was centrifuged at 200,000 g for 2 h (SW60 rotor, Optima LE-80K Ultracentrifuge, Beckman Coulter, CA, USA) to pellet insoluble components. To obtain cytosolic extracts from HeLa or HEK cell lines, cells grown to confluence in 10 cm plates were washed with cold PBS and detached using a cell lifter. Cells were pelleted by 5 min centrifugation at 450 g, and suspended in 100 µl volumes of homogenization buffer. Cells were homogenized with a syringe by repeatedly passing them through a 27 Gauge needle. The homogenate was centrifuged at 10,000 g for 15 min, the supernatant was recovered and centrifuged at 200,000 g for 1 h (TLA55 rotor, Optima Max Ultracentrifuge, Beckman Coulter, CA, USA) to pellet insoluble components.

**Liposome preparation:** All lipids were from Avanti Polar Lipids Inc. (AL, USA) and the concentrations were confirmed by total phosphorus assay (Rouser et al., 1966). Phosphatidylcholine (PC, 1,2 DOPC) or sphingomyelin (SM, porcine brain extract), phosphatidylethanolamine (PE, porcine brain extract), phosphatidylserine (PS, porcine brain extract), cholesterol (free cholesterol), maleimide lipid anchor (18:1 PE-MCC) and PI[4]P (porcine brain extract) or (when indicated) PI[4,5]P<sub>2</sub> (porcine brain extract) were mixed in a molar ratio of 41.5% : 31.5% : 10.5% : 10.5% : 1% : 5%. The incorporation of charged lipids into liposomes as well as reproducibility was confirmed by zeta potential measurements (Malvern, ZetaSizer Nano ZS). Where not specifically indicated, liposomes contained PC. For GUV formation, DiI-C16 was added in a molar ratio of 0.02%. Lipids were dried with a stream of Nitrogen. The lipid film was rehydrated with coupling buffer (20 mM Hepes pH 7.2, 125 mM potassium acetate, 1 mM EDTA) to a lipid concentration of 2 µmol/ml. Liposomes were formed by extrusion through an 800 nm membrane (PC MB 19 mm, 0.8 µm, Whatman, GE Lifesciences, Germany) using a Mini-Extruder from Avanti Polar Lipids Inc. (AL, USA). Coupling of the gE/gpI cd peptide to freshly prepared 18:1 PE-MCC containing liposomes took place at room temperature for 1 h in presence of 1 mM TCEP (tris(2-carboxyethyl)phosphine). The gE/gpI cd peptide (NH<sub>2</sub>-CGKRMRVKAYRVKSPYNQSMYYAGLPVDDFEDSESTDTEE-COOH) was synthesized by EZBiolab (IN, USA). Alternatively, the gE/gpI cd was cloned in a modified pET28 expression plasmid (Niehage et al., 2014) and the 6xHis-MBP--tagged peptide was purified by affinity chromatography. Subsequently, the affinity tag was removed by TEV protease cleavage and the peptide was further purified by size exclusion chromatography.

**Protein recruitment onto liposomes:** Cytosolic extract (protein concentration 4 mg/ml) was supplemented with 100 µM GTPγS, and (when indicated) ATP-regeneration system (1 mM ATP, 10 mM creatine phosphate, 10 µg/ml creatine kinase) and 20 µM latrunculin B. Liposomes were added to a final concentration of about 200 nmol/ml. The mixture was incubated at 37°C for indicated times. Reaction was stopped by addition of 1 ml of cold recruitment buffer. Liposomes were separated from the cytosol mixture by centrifugation (20,000 g for 15 min). Pellets were resuspended in 25 µl of 2X Laemmli buffer, and analyzed by SDS-PAGE and Western blot.

For mass spectrometry analysis, we used 1 ml of mouse brain cytosol (protein concentration 10 mg/ml) and 100 µl liposomes (~100 µmol total lipid). After 25 min at 37°C, the reaction mixture was mixed with 4.5 ml of 65% (w/v) sucrose in recruitment buffer, and then transferred to a 14 ml ultracentrifugation tube. The mixture was overlaid with 5.5 ml of 40% (w/v) sucrose in recruitment buffer, then with 2 ml recruitment buffer, and then centrifuged (12 h, 35,000 RPM, 4°C) in a free-swinging rotor (SW-40), using an Optima LE80 ultracentrifuge. The sucrose interphase containing liposomes was recovered, and liposomes were harvested by centrifugation (20,000g, 15 min, 4°C). Pellets were re-suspended in 25 µl of 2X Laemmli buffer and analyzed by SDS-PAGE.

**Mass spectrometry-based proteomic analysis:** Control and treated samples were separated by SDS-PAGE side-by-side. Gel lanes were cut into 30 slices in parallel fashion. Protein digestion and in-gel <sup>16</sup>O/<sup>18</sup>O-labeling was performed as described (Lange et al., 2010). In brief, gel pieces were incubated



with 100 ng trypsin (Promega, WI, USA) in the presence of H<sub>2</sub>O<sup>18</sup> (97% <sup>18</sup>O, Campro Scientific GmbH, Germany) or H<sub>2</sub>O<sup>16</sup> as indicated, and paired samples were combined immediately before nano-LC-MS/MS analysis. Label-free sample preparation for mass spectrometry was done as described (Czupalla et al., 2006). Peptides were separated on an EASY-nLC nano-HPLC system (Proxeon, Denmark) equipped with a fused silica microcapillary C18 analytical column (3 µm, 100 Å, 10 cm x 75 µm i.d.) directly coupled to the nanoelectrospray source of a LTQ Orbitrap XL mass spectrometer (Thermo Fisher Scientific). Peptides were eluted with a 90 min gradient of 5-50% acetonitrile in 0.1% formic acid at 300 nL/min. Mass spectra were acquired in a data-dependent mode with one MS survey scan (resolution of 60,000) in the Orbitrap and MS/MS scans of the five most intense precursor ions in the LTQ. MS/MS spectra of <sup>16</sup>O/<sup>18</sup>O-labeling experiments were processed and searched against the UniProtKB/SwissProt database (release 56.9, 412,525 sequences, 16,091 *Mus musculus* sequences) using a Mascot server (version 2.2, Matrix Sciences Ltd., UK). Search criteria were: taxonomy, mouse; mass tolerance of precursor and sequence ions, 10 ppm and 0.35 Da, respectively; modifications, cysteine carbamidomethylation, methionine oxidation, serine/ threonine/ tyrosine phosphorylation, and C-terminal <sup>18</sup>O1- and <sup>18</sup>O2-isotope labeling; maximum two missed cleavages. A protein was accepted as identified if the total Mascot score was greater than the significance threshold ( $p < 0.05$ ) and if at least two unique peptides were detected. Based on decoy database searches, the false discovery rate was estimated to be  $< 1\%$ . Quantification was carried out using the Mascot Distiller Quantification Toolbox (version 2.2.1.2, Matrix Sciences) and was based on calculations of at least two unique tryptic peptides. Relative protein ratios were calculated from the intensity-weighted average of all peptide ratios. For most proteins, peptides were detected in separate, adjacent, gel slices. Based on the calculated protein scores, we excluded the gel slices with low scores ( $< 25\%$  of the highest protein score calculated in one gel slice) and low peptide number ( $< 25\%$  of the maximum number). The remaining values (high/low ratios) were averaged to obtain the global peptide ratio (Table S1).

The LC-MS workflow of label-free liposome recruitment experiments has been described in (Niehage et al., 2014). Briefly, samples were fractionated after SDS-PAGE by cutting full lanes into 12 slices, cysteins reduced, carbamidomethylated and proteins in-gel digested by trypsin in a 1:50 ratio. Peptides were separated on a 15 cm reversed-phase column (C18, 15 cm x 75 µm, 2 µm beads of 100-Å pore size; Dionex) within a 60 min gradient from 0.1% formic acid / 5% acetonitrile to 0.1% formic acid / 40% acetonitrile operated by an Ultimate 3000 HPLC system (Dionex). Mass spectrometry was performed with a LTQ Orbitrap XL mass spectrometer (Thermo Scientific), equipped with a nanoESI source (Proxeon). The top eight peaks in the mass spectra (Orbitrap; resolution, 60,000) were selected for fragmentation (CID; normalized collision energy, 35%; activation time, 30 ms, q-value, 0.25) with dynamic exclusion enabled (repeat count, 2; repeat duration, 10 s; exclusion duration, 20 s). MS/MS spectra were acquired in the LTQ in centroid mode. Proteins were identified using the MaxQuant software package version 1.2.2.5 (MPI for Biochemistry, Germany) (Cox and Mann, 2008) and UniProt database version 01/2012. Carbamidomethylation of cysteine was chosen as a fixed modification; acetylation of the N-terminus, deamidation of asparagine and oxidation of methionine as variable modifications. The MaxQuant result file was further processed in Perseus version 1.2.0.13 (MPI for Biochemistry, Germany). Proteins with at least one unique and two razor peptides were kept when present in at least two of three replicates. A t-test was performed with a threshold value of 0.001 and a slope value of the threshold curve of 0.2.

Data analysis of label-free experiments was done using MaxQuant version 1.2.2.5 (Cox and Mann, 2008). Peak lists were searched against a database containing 20,253 entries from the UniProtKB/Swiss-Prot human database (release 2011\_02) and 255 frequently observed contaminants as well as reversed sequences of all entries and the search criteria listed above with the following exceptions: mass accuracy, 6 ppm and 0.5 Da for precursor ion and fragment ion mass tolerance, respectively; fixed and variable modifications, cysteine carbamidomethylation and methionine oxidation, respectively. Peptide identifications were accepted based on their posterior error probability until less than 1% reverse hits were retained while protein false discovery rates were  $< 1\%$ . Proteins were considered if at least two peptides were identified. All Mass Spectrometry data will be made available upon request.

**Statistical Analyses** were performed using Microsoft Excel for Mac and StatPlus Mac (AnalystSoft Inc., CA, USA). Data are shown as mean  $\pm$  SD or median  $\pm$  SD, and p-values were calculated using one-way Anova (\* $p \leq 0.05$ , \*\*  $p \leq 0.005$ ).

**Gene set enrichment analysis (GSEA)** uses statistical methods (hypergeometric distribution) to establish if components of a particular subcellular/molecular pathway are over-represented among a defined set of genes. We performed GSEA using the software provided by the Broad Institute, CA, USA (<http://software.broadinstitute.org/gsea/index.jsp>) (Subramanian et al., 2005, Mootha et al., 2003).

**Thin Layer Chromatography (TLC) of lipids.** After the incubation of liposomes with mouse brain cytosol (protein concentration 4 mg/ml) for indicated times, lipids were immediately extracted using chloroform/methanol (10:1 v/v) (Folch et al., 1957), incubated for 20 min on ice, and centrifuged (5000 g, 4°C, 4 min). The upper, aqueous phase was re-extracted with chloroform/methanol/acetone/1 M HCl (2:1:0.5:0.1 v/v) (Dawson and Eichberg, 1965). All samples were kept on ice during the entire extraction procedure. The respective organic phases were pooled and subsequently evaporated under a nitrogen stream. Samples were then dissolved in 20 µl chloroform/methanol/acetone/1 M HCl (2:1:0.5:0.1 v/v) and loaded on silica gel 60 HPTLC plates (Merck KGaA, Germany) pre-coated with potassium oxalate (Gonzalez-Sastre and Folch-Pi, 1968). As mobile phase, we used either hexane/diethyl ether/acetic acid (80:20:1 v/v) for non-polar lipids, or chloroform/methanol/acetone/acetic acid/water (46:15:17:14:8 v/v) for polar lipids. Lipids were stained with 0.5 % primulin (in acetone/water 8/2 v/v) (White et al., 1998) and visualized in a laser scanner (Typhoon 9410, Amersham Biosciences) with a 457 nm excitation wavelength.

**Mass spectrometry-based lipidomics.** Synthetic lipid standards were purchased from Avanti Polar Lipids and Sigma-Aldrich. Other chemicals were of ACS, CHROMASOLV® Plus or LC-MS grade and purchased from Sigma-Aldrich. Lipids were extracted with methyl-tert-butyl ether (MTBE) as described (Matyash et al., 2008). After incubation with mouse brain cytosol (4 mg/ml) for indicated time points, liposomes in solution (200 µl total volume) were immediately added into a 2 ml safe-lock Eppendorf tube together with 1 ml MTBE /methanol (10:3; v:v) mixture, containing internal standards: 680 pmol SM 18:1:1/12:0; 1310 pmol PC 12:0-13:0; 421 pmol PE 12:0-13:0; 318 pmol PS 12:0-13:0; 847 pmol FC-D7; 55 pmol PI[4]P4 16:0-16:0 and 173 pmol DAG-D5 17:0-17:0. The mixtures were shaken for 90 min (4°C) and centrifuged for 5 min at 13,400 rpm at 4°C. The upper organic phase was transferred to a glass vial and dried under vacuum. Prior to their analysis by mass spectrometry, lipid extracts were dissolved in isopropanol/methanol/chloroform mixture (4:2:1, v:v:v) with 7.5 mM ammonium formate to a final concentration of 20 µM. Shotgun lipidomics analyses were performed on a Q Exactive mass spectrometer (Thermo Fisher Scientific, Germany) equipped with a robotic nanoflow ion source TriVersa NanoMate (Advion BioSciences, Ithaca, NY). Samples were analyzed in technical replicates by broad band FT MS+ (t = 30s, range of m/z 350-1100, mass resolution  $R_{m/z200} = 140.000$ , AGC =  $3 \cdot 10^6$ ), targeted SIM FT MS+ (t = 150s, m/z 400-1000, isolation width = 20 Th, step size = 10 Th,  $R_{m/z200} = 140.000$ , AGC =  $5 \cdot 10^4$ ) followed by targeted HCD FT MS/MS (isolation width = 1 Th,  $R_{m/z200} = 140.000$ , AGC =  $2 \cdot 10^4$ ). Normalized collision energy for targeted MS/MS of PI[4]P, cholesterol and DAG was set to 12% and 20%, respectively. Lipid species were quantified from pre-processed stitched SIM spectra and targeted HCD FT MS/MS using LipidXplorer software (Herzog et al., 2011) PC, PE, SM, PS were quantified by FT MS; free cholesterol, DAG and PI[4]P by HCD FT MS/MS.

**Preparation of Giant Unilamellar Vesicles (GUVs).** GUVs were generated from liposomes by the electro-swelling method (Bacia et al., 2004). 10–20 µl of liposomes were dried onto two Indium tin oxide-slides (Präzisions Glas & Optik, Germany) by 20 min desiccation under vacuum. Separated by a rubber ring spacer, the slides were assembled together, and 600 µl of 330 mM sucrose were added between the slides. GUVs were formed from liposomes by applying an alternating electric field (10 Hz, sinusoidal wave, 1.8 V) for 2 h, using a Voltcraft 8202 1-channel-function generator (Conrad Electronic, Germany). Subsequently, the GUV containing solution was recovered and diluted in 2 volumes of recruitment buffer. GUVs were allowed to settle down for 30 min, and 200 µl GUV suspension were recovered from the bottom of the tube.

**GUV recruitment assays.** Cytosol (4 mg/ml) from cells expressing the GFP-tagged protein of interest was clarified by centrifugation at 150,000 g for 30 min. ATP-regeneration system or inhibitors were added as indicated, and the mixture was placed into the wells of an 8-well Lab-Tek glass bottom chamber (Nunc, Germany, pre-coated with 10 mg/ml BSA at 37°C for 1 h.) 10 µl GUV suspension was added to 100 µl of cytosol, and mixed by pipetting up and down. After 20 min incubation at 37°C, the GUVs were analyzed by confocal microscopy.

**Microscopy:** For microscopy of fixed samples, cells were seeded on 12 mm, No 1.5 glass coverslips (Menzel GmbH, Thermo Scientific, Germany). Cells were washed with PBS, fixed with 4% (w/v) paraformaldehyde in PBS (15 min at room temperature), permeabilized with ice cold 0.1% (v/v) Triton X-100 in PBS (5 min) and then blocked with 3% (w/v) BSA in PBS (20-30 min). For labeling with anti-PI[4,5]P2 and anti-PIP5K1A, cells were washed during all steps with TBS, fixed with 4% (w/v) paraformaldehyde in PBS (15 min), permeabilized with 0.5% saponin (Sigma) for 15 min at room temperature, and blocked with 3% (w/v) BSA in PBS. Cells were incubated with the primary antibody (1 hour at room temperature), washed 3 times (5 min) with PBS, and then labeled with secondary antibodies and DAPI (30 min at room temperature). Subsequently cells were mounted on microscopy slides using MOWIOL (Calbiochem/Merck). Cells were imaged using a LSM 700 or a LSM780 microscope equipped with a 63x 1.4 numerical aperture (NA) or a 100x 1.45 NA Plan-Apochromat objective (Carl Zeiss Microimaging, Germany). For quantifying PI[4,5]P2 on GFP-MPR TGN membranes, 3D renditions were obtained from 0.5  $\mu$ m Z-sections using the ImageJ 3D Viewer plugin (volume view) (Rasband, W.S., ImageJ, U. S. National Institutes of Health, Bethesda, Maryland, USA, <http://imagej.nih.gov/ij/>, 1997-2016). The GFP-MPR positive area was selected, and the number and area of objects within this area was calculated. GUVs were analyzed with 40x 1.2 NA water-immersion objective (Carl Zeiss Microimaging). For quantifying p34-Arc on GFP-MPR TGN membranes, 3D renditions were obtained from 0.5  $\mu$ m Z-sections using the Volocity software (PerkinElmer, MA, USA). The number of objects within the GFP-MPR positive TGN volume was calculated using Image J. The maximum projection of the GFP-MPR in the Z-stack was used to select a region of interest within each image. The number of objects within this region was calculated for the entire Z-stack using the Object Counter 3D plugin (Bolte and Cordelières, 2006). The Golgi region was identified using GM130 staining, and the area covered by GFP-MPR in this region, as well as the total cell area were measured using ImageJ. The ratio between the two areas was calculated.

For live cell imaging, 60,000 – 120,000 cells were plated on 3.5 cm No. 1.5 glass bottom dishes (MaTek Corporation, MA, USA). Before imaging, cells were washed with PBS and DMEM without phenol red was added. High-speed time-lapse microscopy was performed with either an AFLX6000 microscope equipped with an EMCCD detector, with temperature, CO<sub>2</sub> and humidity control, using a 63x 1.4 NA or a 100x 1.4 NA oil-immersion objective (Leica Microsystems, Germany), or with an Axiovert 200 M with temperature, CO<sub>2</sub> and humidity control and a 63x 1.4 NA Plan-Apochromat objective (Carl Zeiss Microimaging). Movies S3 and 4 were acquired using spinning disk microscopy (PICT-IBiSA Imaging Facility, Paris, France). We used a fast scanning confocal with a spinning disk system mounted on the Ti Eclipse Nikon microscope equipped with perfect focus system and a CCD Coolsnap HQ2 camera and a 100X, 1.45 NA objective (Nikon, Japan).

**RAC1 activation assay.** GFP-MPR expressing cells were treated with the indicated siRNAs (20 nM) and Interferin. After 3 days, cells were detached and transferred on 10 cm plates coated (30 min, 37°C) with 5  $\mu$ g/ml fibronectin (Applichem, Germany). After 3.5 -4h, cells were washed two times with 5 ml ice-cold washing buffer (25 mM Tris pH 7.5, 30 mM MgCl<sub>2</sub>, 40 mM NaCl), then cells from each plate were collected in 250  $\mu$ l lysis buffer: 50 mM TrisHCl, pH 7.2, 1% (w/v) Triton X-100, 300 mM NaCl, 10 mM MgCl<sub>2</sub>, complete protease inhibitors (Roche, Germany), 1 mM PMSF, 8 mM sodium fluoride, 2 mM sodium orthovanadate, 2 mM sodium pyrophosphate (Sigma-Aldrich). Cells were lysed by passing through a 27G needle. Lysates were centrifuged at 14,000 g for 5 min, and the supernatant was collected. 10  $\mu$ l PAK-GST beads (1 mg/ml, Cytoskeleton Inc., CO, USA) were added to each tube. Samples were incubated on the rotator (1h, 4°C), beads were collected by centrifugation (8000 g, 1min, 4°C), washed twice with 500  $\mu$ l washing buffer with protease and phosphatase inhibitors, re-suspended in 25  $\mu$ l 4X Laemmli buffer and analyzed by SDS-PAGE and Western blot.

## SUPPLEMENTAL REFERENCES

- BACIA, K., SCHERFELD, D., KAHYA, N. & SCHWILLE, P. 2004. Fluorescence correlation spectroscopy relates rafts in model and native membranes. *Biophys J*, 87, 1034-43.
- BALLA, A., TUYMETOVA, G., TSIOMENKO, A., VARNAL, P. & BALLA, T. 2005. A plasma membrane pool of phosphatidylinositol 4-phosphate is generated by phosphatidylinositol 4-

- kinase type-III alpha: studies with the PH domains of the oxysterol binding protein and FAPP1. *Mol Biol Cell*, 16, 1282-95.
- BOLTE, S. & CORDELIÈRES, F. P. 2006. A guided tour into subcellular colocalization analysis in light microscopy. *J Microsc*, 224, 213-32.
- COX, J. & MANN, M. 2008. MaxQuant enables high peptide identification rates, individualized p.p.b.-range mass accuracies and proteome-wide protein quantification. *Nat Biotechnol*, 26, 1367-72.
- CZUPALLA, C., MANSUKOSKI, H., RIEDL, T., THIEL, D., KRAUSE, E. & HOFLACK, B. 2006. Proteomic analysis of lysosomal acid hydrolases secreted by osteoclasts: implications for lytic enzyme transport and bone metabolism. *Mol Cell Proteomics*, 5, 134-43.
- DAWSON, R. M. & EICHBERG, J. 1965. Diphosphoinositide and triphosphoinositide in animal tissues. Extraction, estimation and changes post mortem. *Biochem J*, 96, 634-43.
- FOLCH, J., LEES, M. & SLOANE STANLEY, G. H. 1957. A simple method for the isolation and purification of total lipides from animal tissues. *J Biol Chem*, 226, 497-509.
- GALLEGOS, L. L., KUNKEL, M. T. & NEWTON, A. C. 2006. Targeting protein kinase C activity reporter to discrete intracellular regions reveals spatiotemporal differences in agonist-dependent signaling. *J Biol Chem*, 281, 30947-56.
- GONZALEZ-SASTRE, F. & FOLCH-PI, J. 1968. Thin-layer chromatography of the phosphoinositides. *J Lipid Res*, 9, 532-3.
- HERZOG, R., SCHWUDKE, D., SCHUHMANN, K., SAMPAIO, J. L., BORNSTEIN, S. R., SCHROEDER, M. & SHEVCHENKO, A. 2011. A novel informatics concept for high-throughput shotgun lipidomics based on the molecular fragmentation query language. *Genome Biol*, 12, R8.
- HUBNER, N. C., BIRD, A. W., COX, J., SPLETTSTOESSER, B., BANDILLA, P., POSER, I., HYMAN, A. & MANN, M. 2010. Quantitative proteomics combined with BAC TransgeneOmics reveals in vivo protein interactions. *J Cell Biol*, 189, 739-54.
- KAWANO, M., KUMAGAI, K., NISHIJIMA, M. & HANADA, K. 2006. Efficient trafficking of ceramide from the endoplasmic reticulum to the Golgi apparatus requires a VAMP-associated protein-interacting FFAT motif of CERT. *J Biol Chem*, 281, 30279-88.
- LANGE, S., SYLVESTER, M., SCHUMANN, M., FREUND, C. & KRAUSE, E. 2010. Identification of phosphorylation-dependent interaction partners of the adapter protein ADAP using quantitative mass spectrometry: SILAC vs (18)O-labeling. *J Proteome Res*, 9, 4113-22.
- MACHACEK, M., HODGSON, L., WELCH, C., ELLIOTT, H., PERTZ, O., NALBANT, P., ABELL, A., JOHNSON, G. L., HAHN, K. M. & DANUSER, G. 2009. Coordination of Rho GTPase activities during cell protrusion. *Nature*, 461, 99-103.
- MATYASH, V., LIEBISCH, G., KURZCHALIA, T. V., SHEVCHENKO, A. & SCHWUDKE, D. 2008. Lipid extraction by methyl-tert-butyl ether for high-throughput lipidomics. *J Lipid Res*, 49, 1137-46.
- MOOTHA, V. K., LINDGREN, C. M., ERIKSSON, K. F., SUBRAMANIAN, A., SIHAG, S., LEHAR, J., PUIGSERVER, P., CARLSSON, E., RIDDERSTRALE, M., LAURILA, E., HOUSTIS, N., DALY, M. J., PATTERSON, N., MESIROV, J. P., GOLUB, T. R., TAMAYO, P., SPIEGELMAN, B., LANDER, E. S., HIRSCHHORN, J. N., ALTSHULER, D. & GROOP, L. C. 2003. PGC-1alpha-responsive genes involved in oxidative phosphorylation are coordinately downregulated in human diabetes. *Nat Genet*, 34, 267-73.
- NIEHAGE, C., STANGE, C., ANITEI, M. & HOFLACK, B. 2014. Liposome-based assays to study membrane-associated protein networks. *Methods Enzymol*, 534, 223-43.
- ROUSER, G., SIAKOTOS, A. N. & FLEISCHER, S. 1966. Quantitative analysis of phospholipids by thin-layer chromatography and phosphorus analysis of spots. *Lipids*, 1, 85-6.
- ROZELLE, A. L., MACHESKY, L. M., YAMAMOTO, M., DRIESSENS, M. H., INSALL, R. H., ROTH, M. G., LUBY-PHELPS, K., MARRIOTT, G., HALL, A. & YIN, H. L. 2000. Phosphatidylinositol 4,5-bisphosphate induces actin-based movement of raft-enriched vesicles through WASP-Arp2/3. *Curr Biol*, 10, 311-20.
- STAUFFER, T. P., AHN, S. & MEYER, T. 1998. Receptor-induced transient reduction in plasma membrane PtdIns(4,5)P2 concentration monitored in living cells. *Curr Biol*, 8, 343-6.
- SUBRAMANIAN, A., TAMAYO, P., MOOTHA, V. K., MUKHERJEE, S., EBERT, B. L., GILLETTE, M. A., PAULOVICH, A., POMEROY, S. L., GOLUB, T. R., LANDER, E. S. & MESIROV, J. P. 2005. Gene set enrichment analysis: a knowledge-based approach for interpreting genome-wide expression profiles. *Proc Natl Acad Sci U S A*, 102, 15545-50.
- SZENTPETERY, Z., VARNAI, P. & BALLA, T. 2010. Acute manipulation of Golgi phosphoinositides to assess their importance in cellular trafficking and signaling. *Proc Natl Acad Sci U S A*, 107, 8225-30.

- WAGURI, S., DEWITTE, F., LE BORGNE, R., ROUILLE, Y., UCHIYAMA, Y., DUBREMETZ, J. F. & HOFLACK, B. 2003. Visualization of TGN to endosome trafficking through fluorescently labeled MPR and AP-1 in living cells. *Mol Biol Cell*, 14, 142-55.
- WHITE, T., BURSTEN, S., FEDERIGHI, D., LEWIS, R. A. & NUDELMAN, E. 1998. High-resolution separation and quantification of neutral lipid and phospholipid species in mammalian cells and sera by multi-one-dimensional thin-layer chromatography. *Anal Biochem*, 258, 109-17.



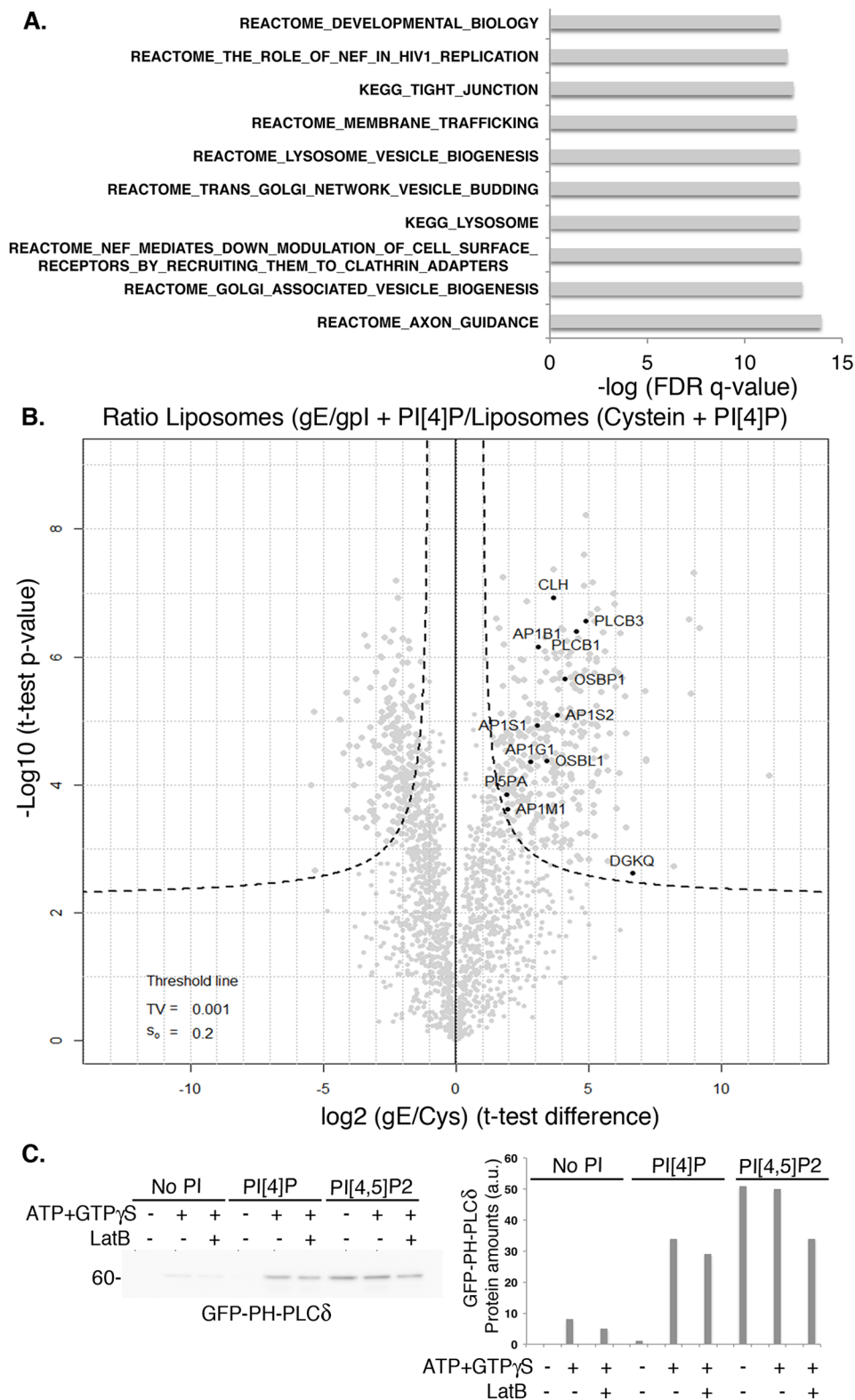


**Fig. S1. Protein recruitment on clathrin/AP-1 coated membranes.** Related to Figure 1, Table S1 Table S2, and Figure 4. (A) Pathway enrichment of the proteins enriched on flat membranes (-ATP) was calculated using GSEA (see also Fig. 1D, Table S1). The False Discovery Rate (FDR)  $q$ -value was calculated for each set. (B) Volcano plot of proteins enriched on liposomes containing AP-1 selective gE/gPI cd peptide compared to control liposomes (Table S2). PI[4]P and PC containing liposomes modified with either gE/gPI cd peptide or cysteine as control, were incubated with mouse brain cytosol in presence of GTP $\gamma$ S and then purified by floatation. Label free quantification of bound proteins was performed (Niehage et al., 2014). Logarithmic ( $\log_2$ ) ratios of protein intensities in the (gE/gPI)/Cys are shown on the X-axis, and the negative logarithmic ( $\log_{10}$ )  $p$ -values of the  $t$ -test from triplicates on the Y-axis;  $TV$ ,  $s_0$ , represent threshold values (Hubner et al., 2010). Proteins significantly enriched gE/gPI cd peptide liposomes appear above the threshold line on the upper right. (C) Liposomes containing the gE/gPI cd peptide, SM, and no PI, PI[4]P or PI[4,5]P2 were incubated with cytosol of HEK cells expressing GFP-PLC $\delta$ -PH for 15 min, in the indicated conditions. Lipid-binding probe recruitment on liposomes was analyzed by Western blot using anti-GFP antibodies (see Fig. 4A, B). Band intensities were measured using ImageJ and the mean intensities were plotted.

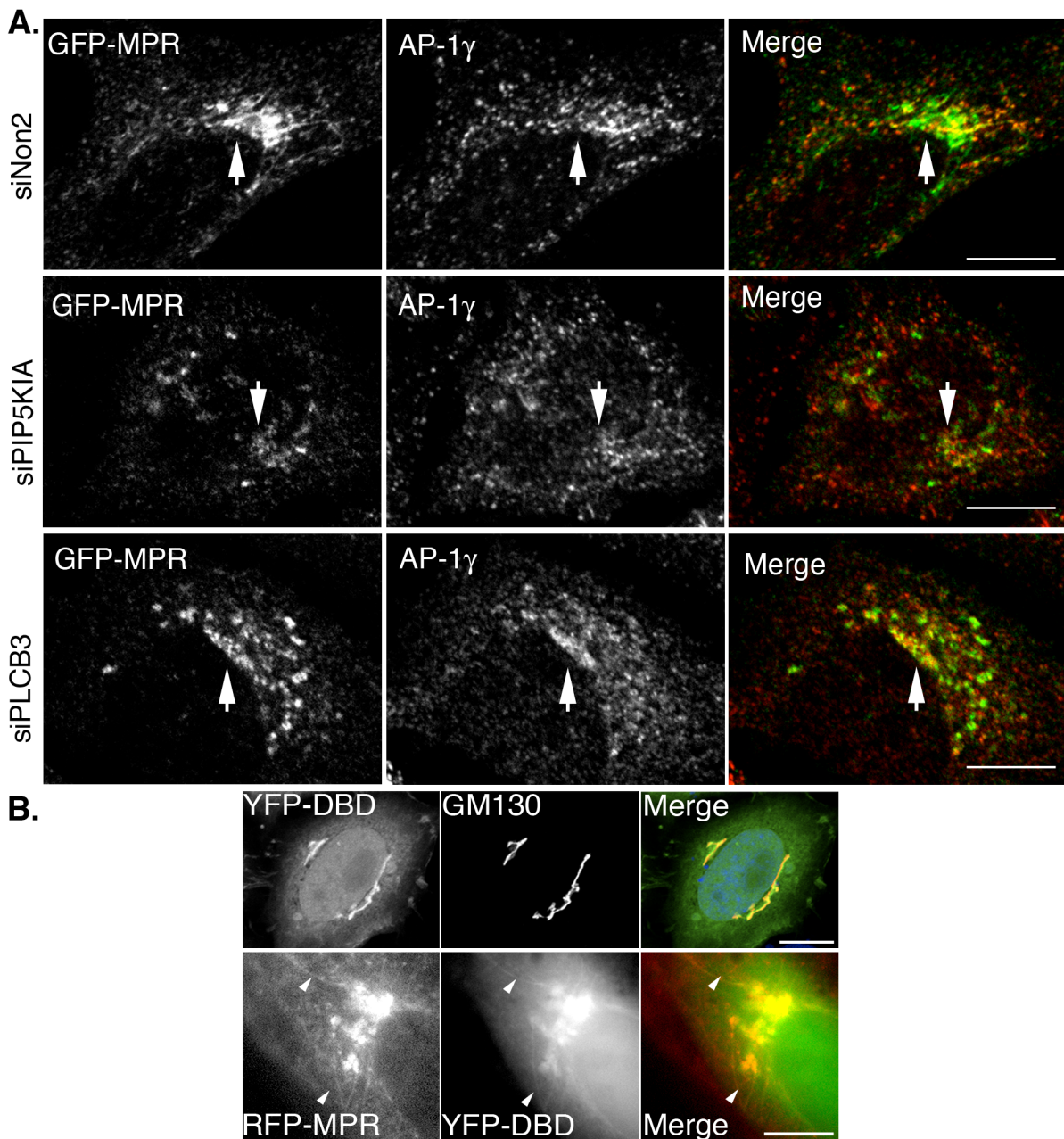


**Fig. S2. Knockdowns of PIP5K1A and PLCB3 affect the morphology of the AP-1 coated compartment.** Related to Figure 2 and Figure 3. (A) HeLa cells stably expressing GFP-MPR were treated with indicated siRNAs for 72 h, fixed and co-labeled with anti-AP-1 $\gamma$  (red). Arrows indicate AP-1 $\gamma$  coated GFP-MPR structures. (B) HeLa cells were transfected with YFP-DBD for 24 h, fixed and co-labeled with anti-GM130 (red, upper panel), or co-transfected with YFP-DBD and RFP-CIMPR (lower panel). Arrowheads indicate TGN-derived MPR positive tubules with bound YFP-DBD (lower panel). Scale bars, 10  $\mu$ m.

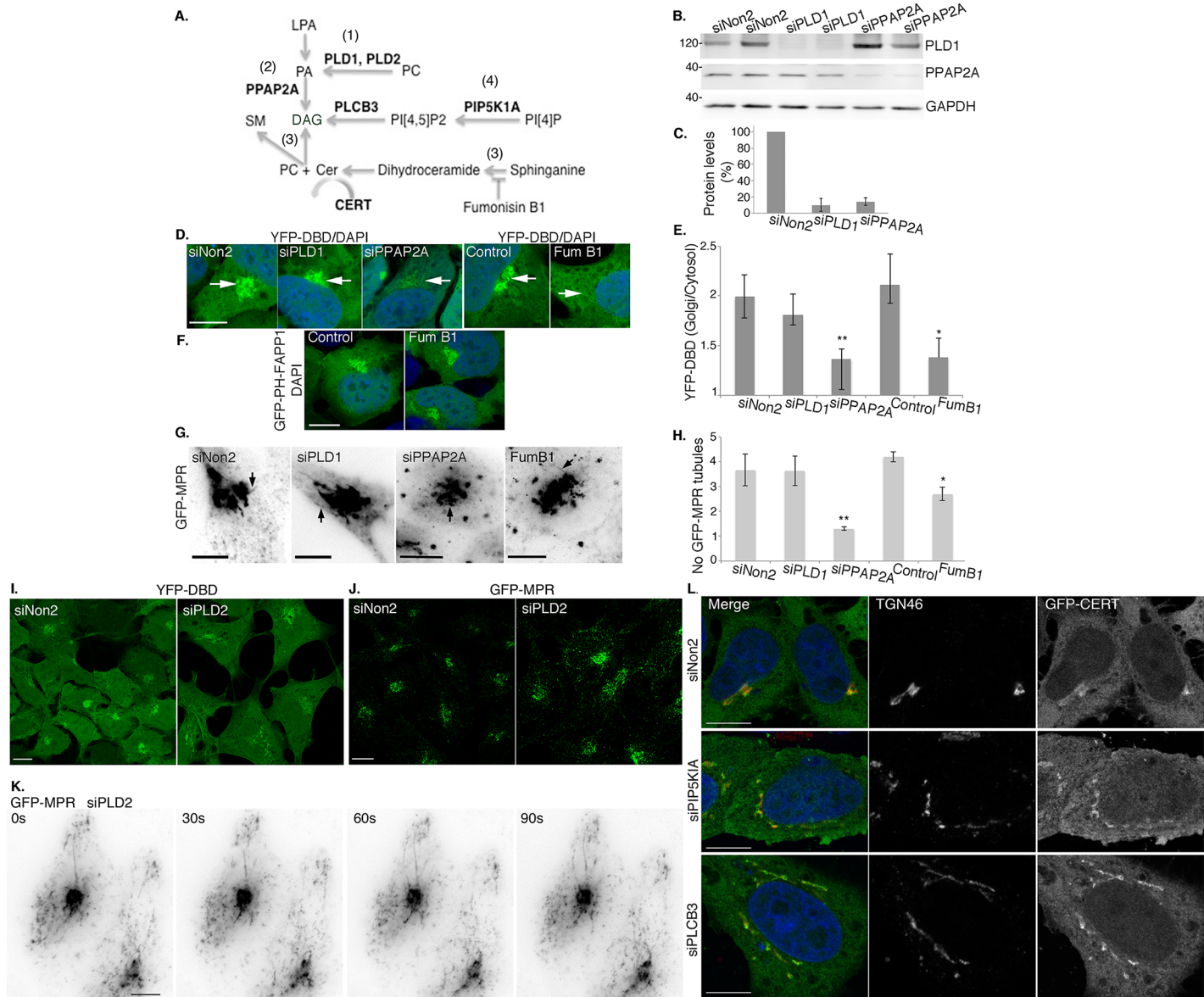


**Fig. S3. DAG production on Golgi membranes.** Related to Figure 3. (A) Metabolic pathways controlling DAG production on Golgi membranes. (1) PLD1 hydrolyzes PC to PA, which is (2) transformed by phosphatases (i.e. PPAP2A) into DAG. (3) DAG and SM are synthesized from PC and ceramide, a reaction blocked by fumonisins B1. (4) PIP5K1A synthesizes, from PI[4]P, PI[4,5]P2 that is hydrolyzed by PLCB3 to form DAG and IP3. (B) GFP-MPR-expressing cells were treated with the indicated siRNAs for 72 h. Knockdown efficiencies were analyzed by Western blot with anti-PLD1, anti-PPAP2A and anti-GAPDH antibodies. (C) Protein levels were quantified using Image J and are shown relative to control siNon2 ( $n = 3$  independent experiments). (D) HEK cells stably expressing YFP-DBD were treated with the indicated siRNAs for 72 h, or with 25  $\mu\text{g/ml}$  of fumonisins B1 for 24 h, then fixed and analyzed using confocal fluorescence microscopy. (E) Fluorescence intensities of YFP-DBD were measured in the Golgi area and in the cytosol using ImageJ. The Golgi/cytosol ratios are shown ( $n \geq 3$ ; \*\* $p$ -value  $< 0.001$ ; \* $p$ -value  $< 0.05$ ,  $\geq 50$  cells/condition). (F) HEK cells stably expressing the GFP-tagged PH domain of FAPP1 were treated with 25  $\mu\text{g/ml}$  fumonisins B1 for 24 h. Cells were fixed and analyzed using confocal fluorescence microscopy.  $N = 3$ . (G) GFP-MPR-expressing cells were incubated with the indicated siRNAs for 72 h, or with 25  $\mu\text{g/ml}$  fumonisins B1 for 24 h and monitored using live cell imaging (2 min, 0.5 s per frame; Movie S2). (H) The number of TGN-derived tubules formed during 2 min per cell was quantified ( $n = 3$ ; \*\* $p$ -value  $< 0.001$ ; \* $p$ -value  $< 0.01$ ,  $> 50$  cells/condition). Data are shown as mean  $\pm$  SD. (I, J) HEK cells expressing YFP-DBD (I) and GFP-MPR expressing HeLa cells (J) were incubated with control siNon2 or siPLD2 for 72 h, fixed and analyzed by confocal microscopy. (K) GFP-MPR (black) expressing cells incubated with control siNon2 or siPLD2 for 72 h were analyzed by time-lapse microscopy (2 min, 0.5 s per frame). Images were inverted;  $n = 2$  independent experiments in duplicate,  $> 64$  cells/condition. (L) HeLa cells were treated with the indicated siRNAs for 48 h, then transfected with GFP-CERT. After 24 h, cells were fixed and co-labeled with anti-TGN46 (red). Scale bars, 10  $\mu\text{m}$ .



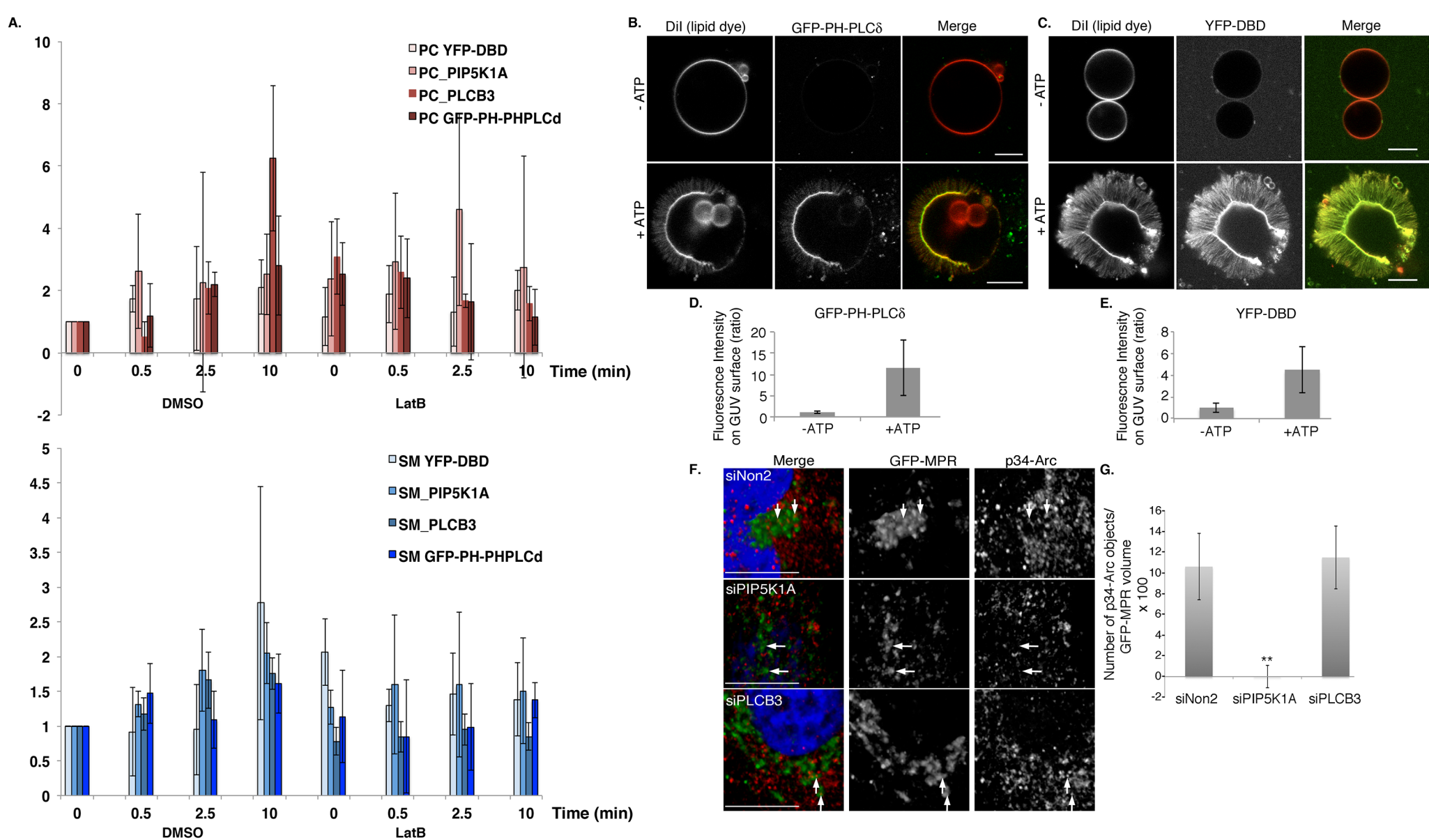


**Fig. S4. Analysis of lipid modifications on artificial membranes, and of ARP2/3-dependent actin polymerization in cells.** Related to Figure 4 and Figure 5. (A) Quantification of data in Fig. 4A-B. Proteins recruited on liposomes containing PC (upper panel) or SM (lower panel) were analyzed by Western blotting, and protein amounts were quantified using ImageJ ( $n = 3-4$  independent experiments). (B-E) GUVs containing PC, the gE/gpI cd peptide and PI[4]P were incubated for 20 min with cytosol from HEK cells stably expressing (B, D) GFP-PLC $\delta$ -PH or (C, E) YFP-DBD, GTP $\gamma$ S and with or without ATP. (D, E) Fluorescence intensities on the GUV surface (25 GUVs per condition) were quantified and are shown as ratios relative to control (-ATP) values (mean  $\pm$  SD). (F, G) GFP-MPR expressing HeLa cells treated with the indicated siRNAs were co-labeled with anti-p34-Arc (red). Z-series of 0.5  $\mu$ m optical sections were acquired. Images represent a 3D rendition of Z-stacks. (G) The number of p34-Arc-positive objects localized in the GFP-MPR region was calculated in the entire stack and shown as (Number of p34-Arc objects/GFP-MPR volume)\*100, median  $\pm$ SD ( $n = 4$  independent experiments, \*\*p-value = 0.002, > 64 cells/condition). GUVs and cells were analyzed by confocal microscopy. Scale bars, 10  $\mu$ m.

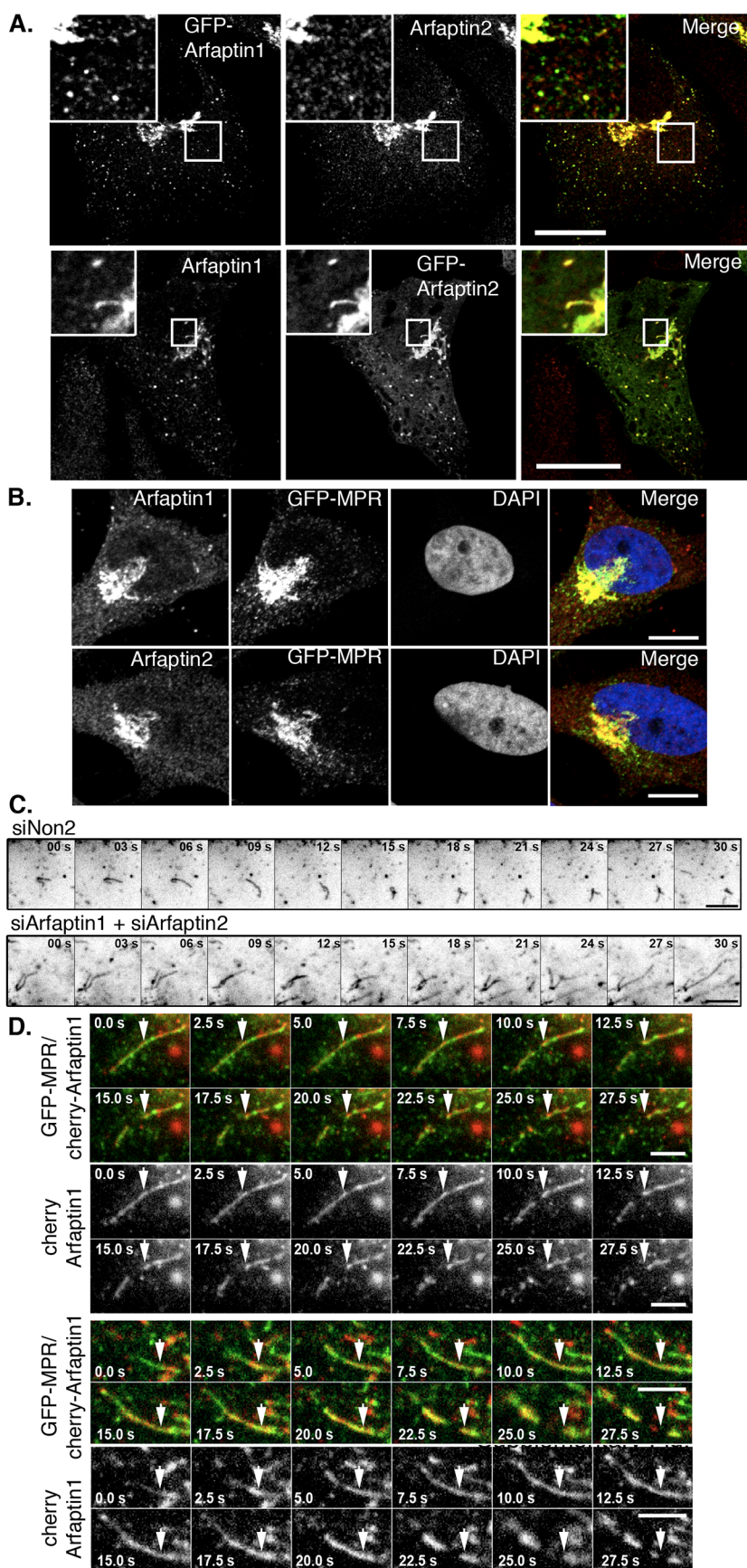


**Fig. S5. Localization and dynamics of arfaptin 1/2.** Related to Figure 6. (A) HeLa cells were transfected with GFP-arfaptin-1 and labeled with anti-arfaptin-2 antibodies (red), or were transfected GFP-arfaptin-2 and labeled with anti-arfaptin-1 antibodies (red). (B) GFP-MPR cells were labeled with anti-arfaptin-1 or anti-arfaptin-2 antibodies (red). (C) GFP-MPR cells were treated with siRNAs targeting both arfaptin-1 and 2. Representative montages (30 s; 3 s interval) show the dynamics of peripheral tubular carriers. (D) Dynamics of peripheral tubular carriers was studied by time-lapse microscopy in HeLa cells co-transfected with GFP-MPR and mCherry-arfaptin-1. Representative montages (30 s, 2.5 s interval) show carrier fragmentation coinciding with arfaptin-1 subdomain segregation. Arrows indicate arfaptin 1 accumulation along the tubes at sites of membrane scission. Scale bars, (A, B) 10  $\mu$ m, (C, D) 5  $\mu$ m.